



**HAL**  
open science

## **p57Kip2 acts as a transcriptional corepressor to regulate intestinal stem cell fate and proliferation**

Justine Creff, Ada Nowosad, Anne Prel, Anne Pizzoccaro, Marion Aguirrebengoa, Nicolas Duquesnes, Caroline Callot, Thomas Jungas, Christine Dozier, Arnaud Besson

### ► To cite this version:

Justine Creff, Ada Nowosad, Anne Prel, Anne Pizzoccaro, Marion Aguirrebengoa, et al.. p57Kip2 acts as a transcriptional corepressor to regulate intestinal stem cell fate and proliferation. *Cell Reports*, 2023, 42 (6), 10.1016/j.celrep.2023.112659 . hal-04234646

**HAL Id: hal-04234646**

**<https://hal.science/hal-04234646>**

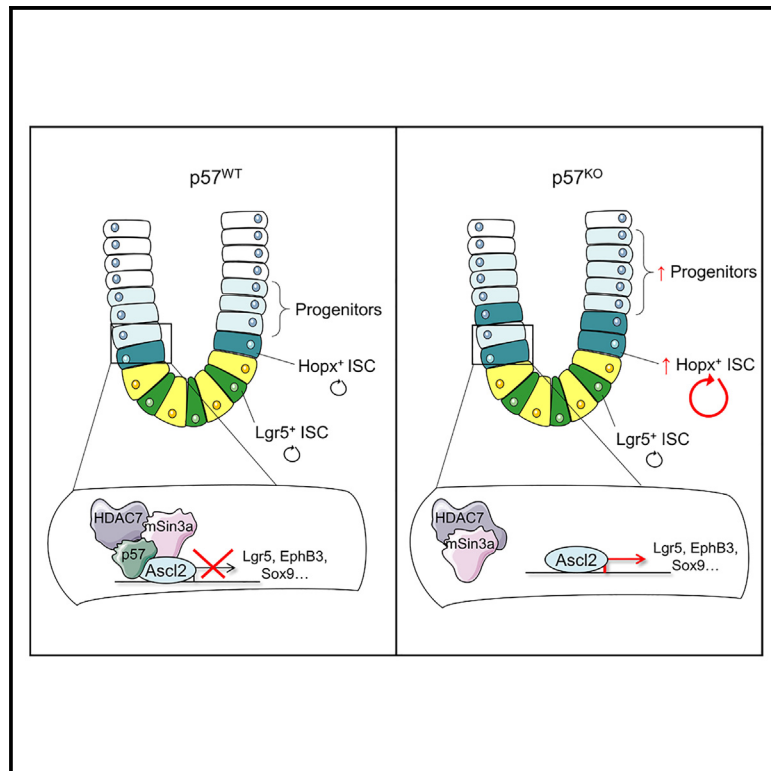
Submitted on 10 Oct 2023

**HAL** is a multi-disciplinary open access archive for the deposit and dissemination of scientific research documents, whether they are published or not. The documents may come from teaching and research institutions in France or abroad, or from public or private research centers.

L'archive ouverte pluridisciplinaire **HAL**, est destinée au dépôt et à la diffusion de documents scientifiques de niveau recherche, publiés ou non, émanant des établissements d'enseignement et de recherche français ou étrangers, des laboratoires publics ou privés.

## p57<sup>Kip2</sup> acts as a transcriptional corepressor to regulate intestinal stem cell fate and proliferation

### Graphical abstract



### Authors

Justine Creff, Ada Nowosad, Anne Prel, ..., Thomas Jungas, Christine Dozier, Arnaud Besson

### Correspondence

arnaud.besson@cnr.fr

### In brief

During intestinal development, p57<sup>Kip2</sup> regulates Hopx<sup>+</sup> intestinal stem cell fate and proliferation in a CDK-independent manner. p57<sup>Kip2</sup> can repress the transcriptional activity of Ascl2 by participating in the recruitment of a corepressor complex on Ascl2 target gene promoters. Loss of p57<sup>Kip2</sup> leads to intestinal stem cell deregulation and dysplasia of the intestinal epithelium.

### Highlights

- p57<sup>Kip2</sup> regulates intestinal stem cell proliferation in a CDK-independent manner
- p57<sup>Kip2</sup> is expressed in Hopx<sup>+</sup> cells during embryonic development
- p57<sup>Kip2</sup> represses the transcriptional activity of Ascl2
- p57<sup>Kip2</sup> participates in the recruitment of a transcriptional corepressor complex



## Article

# p57<sup>Kip2</sup> acts as a transcriptional corepressor to regulate intestinal stem cell fate and proliferation

Justine Creff,<sup>1</sup> Ada Nowosad,<sup>1</sup> Anne Prel,<sup>1</sup> Anne Pizzoccaro,<sup>1</sup> Marion Aguirrebengoa,<sup>1</sup> Nicolas Duquesnes,<sup>1</sup> Caroline Callot,<sup>1</sup> Thomas Jungas,<sup>1</sup> Christine Dozier,<sup>1</sup> and Arnaud Besson<sup>1,2,\*</sup>

<sup>1</sup>Molecular, Cellular and Developmental Biology Department (MCD), Centre de Biologie Intégrative (CBI), University of Toulouse, CNRS, UPS, 31062 Toulouse, France

<sup>2</sup>Lead contact

\*Correspondence: [arnaud.besson@cnrs.fr](mailto:arnaud.besson@cnrs.fr)

<https://doi.org/10.1016/j.celrep.2023.112659>

## SUMMARY

p57<sup>Kip2</sup> is a cyclin/CDK inhibitor and a negative regulator of cell proliferation. Here, we report that p57 regulates intestinal stem cell (ISC) fate and proliferation in a CDK-independent manner during intestinal development. In the absence of p57, intestinal crypts exhibit an increased proliferation and an amplification of transit-amplifying cells and of Hopx<sup>+</sup> ISCs, which are no longer quiescent, while Lgr5<sup>+</sup> ISCs are unaffected. RNA sequencing (RNA-seq) analyses of Hopx<sup>+</sup> ISCs show major gene expression changes in the absence of p57. We found that p57 binds to and inhibits the activity of Ascl2, a transcription factor critical for ISC specification and maintenance, by participating in the recruitment of a corepressor complex to Ascl2 target gene promoters. Thus, our data suggest that, during intestinal development, p57 plays a key role in maintaining Hopx<sup>+</sup> ISC quiescence and repressing the ISC phenotype outside of the crypt bottom by inhibiting the transcription factor Ascl2 in a CDK-independent manner.

## INTRODUCTION

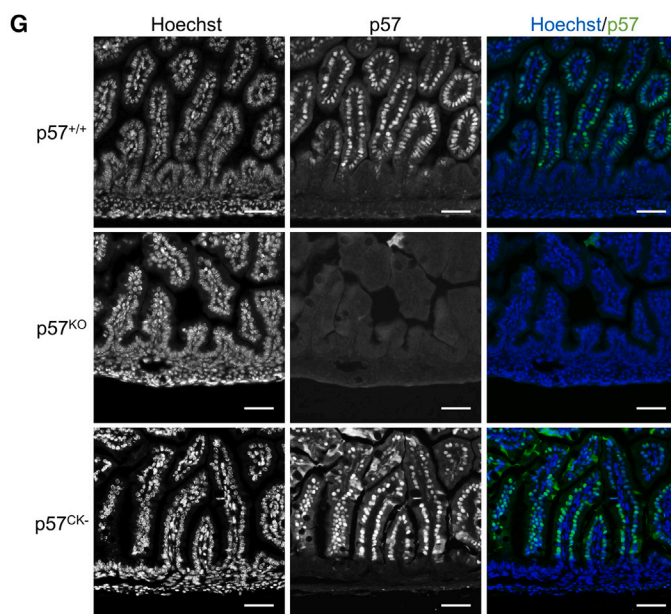
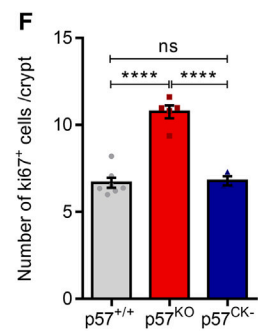
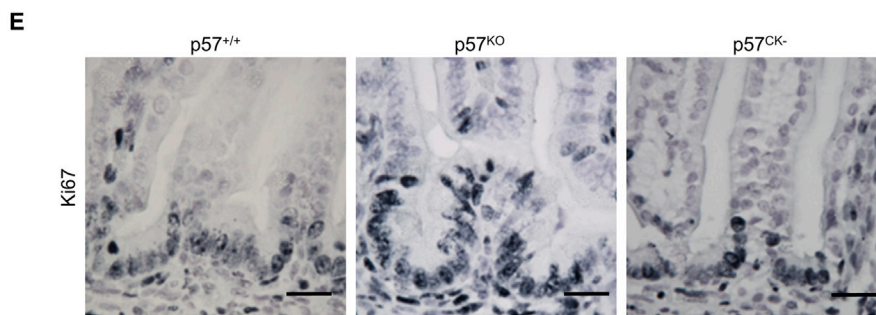
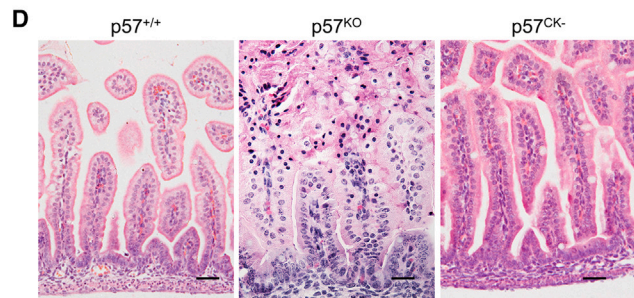
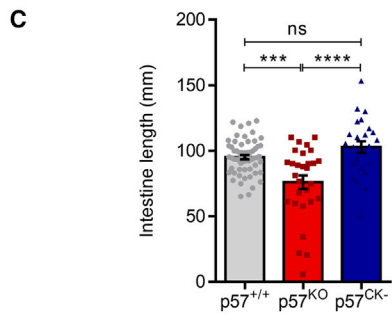
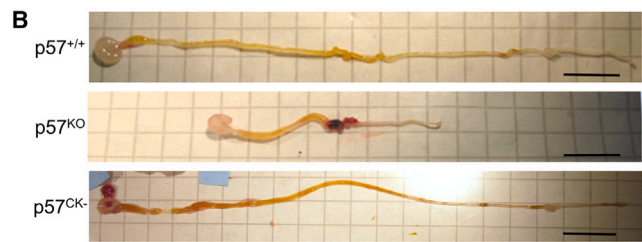
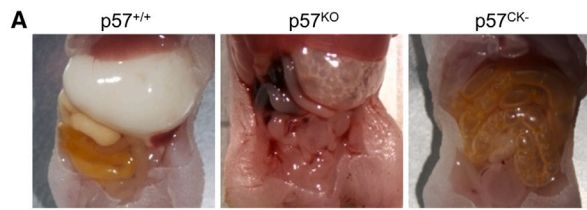
p57<sup>Kip2</sup>, encoded by the *CDKN1C* gene, is a cyclin/CDK inhibitor (CKI) of the Cip/Kip family with p21<sup>Cip1/Waf1</sup> and p27<sup>Kip1</sup>. *CDKN1C* is an imprinted gene and p57 is expressed only from the maternal allele. Through inhibition of CDKs, p57 negatively regulates the cell division cycle, acting as a putative tumor suppressor.<sup>1,2</sup> Unlike other CDK inhibitors, p57 plays a critical role during embryonic development, and the knockout of p57 in mice (p57<sup>KO</sup>) results in perinatal lethality caused by numerous developmental anomalies.<sup>3,4</sup> Some phenotypes of p57<sup>KO</sup> mice resemble features observed in Beckwith-Wiedemann syndrome (BWS).<sup>4,5</sup> Indeed, *CDKN1C* epigenetic repression or mutations are the most frequent causes of BWS.<sup>6,7</sup> Like other Cip/Kip proteins, evidence indicates that, in addition to its CDK-inhibitory function, p57 regulates various biological processes by associating with different protein partners.<sup>2,8</sup> Generation of a knockin mouse model expressing a mutant form of p57 (p57<sup>CK-</sup>) that cannot bind cyclin/CDK complexes has provided genetic evidence for CDK-independent functions of p57 during embryonic development and revealed that BWS is not entirely caused by the loss of CDK inhibition.<sup>5</sup> Importantly, while approximately 30%–40% of p57<sup>KO</sup> mice exhibit intestinal shortening or truncation,<sup>3,9</sup> this phenotype is not observed in p57<sup>CK-</sup> mutant mice,<sup>5</sup> indicating that intestinal development is regulated by p57 in a CDK-independent manner. The mechanism underlying this role of p57 remains unknown. p57 expression was reported in the in-

testinal epithelium, except at the bottom of crypts, where its expression is repressed by the transcription factor Hes1 downstream of Notch receptor signaling.<sup>10</sup> Disruption of Notch1 and -2 results in derepression of p27 and p57 and in premature cell cycle exit and differentiation of intestinal progenitors.<sup>10</sup> More recently, p57 expression was detected in populations of slow-cycling Mex3a<sup>High</sup> and Bmi1<sup>High</sup> intestinal stem cells (ISCs), but its mechanism of action has not been studied.<sup>11,12</sup>

The intestinal epithelium is organized in crypt/villus structures and is one of the most rapidly renewing tissue in the body, with a turnover of 5–7 days.<sup>13,14</sup> Villi are finger-like protrusions covered by a single epithelial layer of post-mitotic, differentiated cells. They are surrounded by crypts, which are invaginations into the mesenchyme where ISCs reside. The rapid renewal of the epithelium is driven by Lgr5<sup>+</sup> ISCs, known as crypt-base columnar cells (CBCs), which localize at the bottom of the crypts, interspersed between Paneth cells.<sup>15</sup> Intestinal development starts around embryonic day 9.5 (E9.5) in mice, with a single-layered pseudostratified epithelium lining the luminal surface of the gut tube.<sup>16</sup> At E14.5, after elongation and thickening of the intestinal tube, major remodeling occurs, resulting in the formation of non-proliferative villi and proliferative intervillous regions by E16.5.<sup>17</sup> Lgr5<sup>+</sup> ISCs first appear at E13.5 and localize to intervillous regions by E16.5.<sup>18,19</sup> Crypts and villi with all intestinal epithelial cell types are fully matured by postnatal day 15 (P15).

Lgr5<sup>+</sup> ISCs divide symmetrically approximately once per day, and, as these cells are progressively excluded from the stem cell





(legend on next page)

zone, they become committed progenitors (secretory or absorptive) called transit-amplifying (TA) cells, which rapidly divide several times before terminally differentiating in the various epithelial cell types lining the intestine.<sup>14,15,20</sup> During differentiation, cells migrate upward from the crypt to the base of villi where they are fully specialized. Once in villi, upward migration continues until cells shed in the intestinal lumen and die by anoikis upon reaching the top of villi.<sup>13,21</sup>

Despite their importance in homeostasis, acute loss of Lgr5<sup>+</sup> ISCs does not compromise epithelial integrity. Indeed, due to their rapid cycling, Lgr5<sup>+</sup> ISCs are sensitive to chemicals, irradiation, or other damage but are regenerated within a few days at the base of the crypt and the epithelium is completely restored. However, constant depletion of Lgr5<sup>+</sup> ISCs abrogates intestinal epithelium renewal, indicating they are the obligatory precursors to all intestinal cell types.<sup>22</sup> While several studies have shown by genetic lineage tracing that Lgr5<sup>+</sup> ISC regeneration can be effected by multiple mature cell types that can dedifferentiate and divide to give new CBCs in the crypt, others have identified rare populations of quiescent reserve stem cells that can restore the Lgr5<sup>+</sup> ISC pool when needed (reviewed elsewhere<sup>14,23,24</sup>). Whether these reserve ISCs are “professional” stem cells or merely committed progenitors that can reverse to a CBC phenotype by dedifferentiation upon crypt injury is still debated.

A number of studies in the adult intestine traced this regenerative capacity to one or more dedicated reserve stem cell pool(s) existing normally in a quiescent or slowly cycling state but able to activate and proliferate actively in case of damage to restore Lgr5<sup>+</sup> ISCs. These reserve ISCs are located near the +4 position and have been identified using different markers, including Bmi1<sup>+</sup>,<sup>25–27</sup> mTert<sup>+</sup>,<sup>28</sup> Hopx<sup>+</sup>,<sup>29</sup> Sox9<sup>High</sup>,<sup>30,31</sup> or a rare population of Clusterin<sup>+</sup> cells.<sup>32</sup> Furthermore, Lgr5<sup>+</sup> and reserve ISCs can restore one another, highlighting a high level of plasticity in the crypt.<sup>29</sup> However, the existence and identity of reserve ISCs remains debated since none of the markers described for reserve ISCs are fully specific of these cells, and at least some Lgr5<sup>+</sup> ISCs express these markers.<sup>33–35</sup> Indeed, while most Lgr5<sup>+</sup> ISCs are rapidly cycling, around 20% are quiescent, and these cells are named label-retaining cells (LRCs).<sup>36</sup> LRCs exhibit both Lgr5<sup>+</sup> and reserve ISCs gene expression signatures, as well as a secretory progenitor gene signature.<sup>36</sup> Consistent with this, another study identified a population of largely quiescent (Ki67<sup>-</sup>) Lgr5<sup>Low</sup> cells located around position +4 whose gene expression signature resembles that described for LRCs.<sup>37</sup> More recently, a Mex3a<sup>High</sup> population was described

as a quiescent Lgr5<sup>+</sup> ISC subpopulation expressing both CBC and +4 markers that is involved in epithelial regeneration.<sup>11</sup> Another mechanism put forth by other studies is that, upon damage, committed secretory (Dil1<sup>+</sup>) and absorptive (Alpi<sup>+</sup>) progenitors can undergo dedifferentiation and act as stem cells to regenerate Lgr5<sup>+</sup> ISCs and the intestinal epithelium.<sup>38,39</sup> Importantly, this dedifferentiation mechanism involves the re-expression and activation of Ascl2, a transcription factor required for Lgr5<sup>+</sup> ISC specification and maintenance.<sup>40–42</sup> Regardless of whether Lgr5<sup>+</sup> ISC recovery after damage is mediated by dedifferentiation of committed progenitors or professional reserve stem cells, how these cells exit quiescence and are mobilized to allow regeneration remains largely unclear.

Here, we investigated the role of the CDK inhibitor p57<sup>Kip2</sup> in intestinal homeostasis during development. Since the “reserve stem cell state” has been defined in the adult intestine after damage to active stem cells and, in the embryo, this definition has not been tested in this conventional context, the term “Hopx<sup>+</sup> ISCs” will be used hereafter to designate putative Hopx<sup>+</sup> reserve ISCs. We find that p57 controls the maintenance of quiescence in a progenitor/stem cell population in a CDK-independent manner. Loss of p57 expression causes increased proliferation in crypts due to amplification of Hopx<sup>+</sup> ISCs and TA cells, while Lgr5<sup>+</sup> ISCs are not affected. Additionally, we found that p57 binds to and inhibits Ascl2 transcriptional activity by participating in the recruitment of a transcriptional corepressor complex containing histone deacetylase 7 (HDAC7) and mSin3a at Ascl2 target gene promoters.

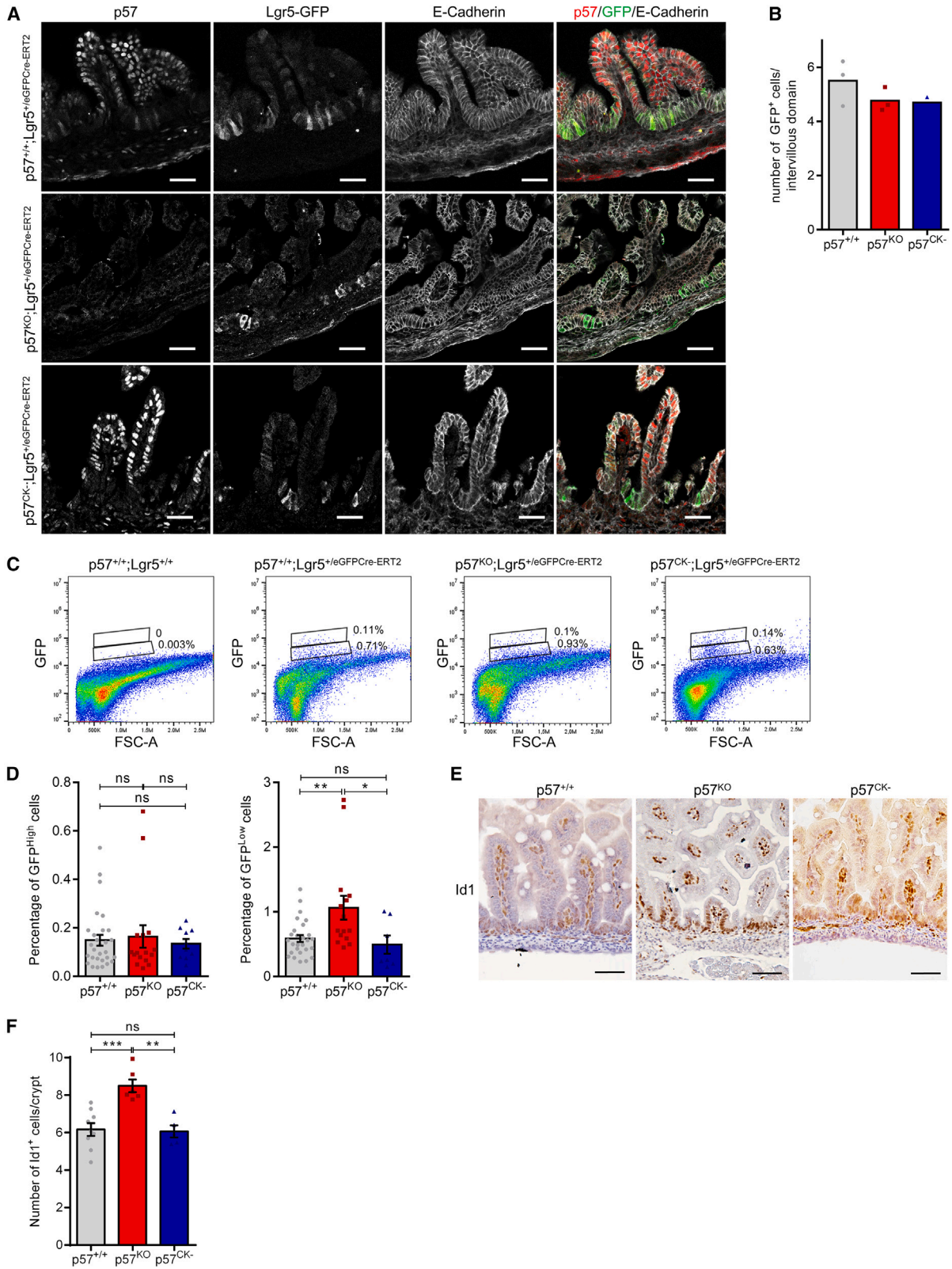
## RESULTS

### p57 plays a critical role in intestinal development in a CDK-independent manner

Approximately 30%–40% of p57<sup>KO</sup> mice exhibit intestinal shortening or truncation at E18.5 (Figures 1A–1C).<sup>3,5,9</sup> Importantly, as reported previously,<sup>5</sup> this phenotype was not observed in p57<sup>CK-</sup> mice, in which p57 cannot bind to and inhibit cyclin-CDK complexes (Figures 1A–1C; Table S1), indicating that p57 plays a critical role in intestinal development independently of CDK inhibition. Histological analyses of H&E-stained intestine sections show that, compared with p57<sup>+/+</sup> and p57<sup>CK-</sup> mice, p57<sup>KO</sup> intestines exhibit a strong disorganization of the intestinal epithelium (Figure 1D), especially in villi, where nuclear morphology was consistent with cell death. This was confirmed by immunostaining against cleaved caspase 3 (Figure S1A). Quantification of proliferative cells by Ki67 immunostaining revealed that p57<sup>KO</sup> intestines exhibit a

### Figure 1. p57 plays a critical role in intestinal development in a CDK-independent manner

- (A) Examples of images of abdomen of p57<sup>+/+</sup>, p57<sup>KO</sup>, and p57<sup>CK-</sup> mice at P1. The presence of air in the gastrointestinal tract of p57<sup>KO</sup> and p57<sup>CK-</sup> mice is caused by cleft palate.
- (B) Examples of images of p57<sup>+/+</sup>, p57<sup>KO</sup>, and p57<sup>CK-</sup> intestines at E18.5. Approximately 30% of p57<sup>KO</sup> mice exhibit intestinal shortening, a phenotype never observed in p57<sup>CK-</sup> mice. Scale bars, 1 cm.
- (C) Intestine length at E18.5 in p57<sup>+/+</sup> (n = 60), p57<sup>KO</sup> (n = 29), and p57<sup>CK-</sup> (n = 25) embryos. Graph shows means ± SEM. One-way ANOVA; ns, p > 0.05; \*\*\*p ≤ 0.001; \*\*\*\*p ≤ 0.0001.
- (D) Representative images of H&E-stained intestine sections from E18.5 embryos showing intestinal epithelium alterations in p57<sup>KO</sup> mice.
- (E) Representative images of Ki67 immunohistochemistry (gray) of intestine sections from p57<sup>+/+</sup>, p57<sup>KO</sup>, or p57<sup>CK-</sup> E18.5 embryos.
- (F) Quantification of Ki67<sup>+</sup> cells per intervillous domain from p57<sup>+/+</sup> (n = 7), p57<sup>KO</sup> (n = 5), and p57<sup>CK-</sup> (n = 3) E18.5 embryos as described in (E). Graph shows means ± SEM. One-way ANOVA; ns, p > 0.05; \*\*\*\*p ≤ 0.0001.
- (G) Representative images of p57 immunostaining (green) of intestine sections from E18.5 p57<sup>+/+</sup>, p57<sup>KO</sup>, and p57<sup>CK-</sup> embryos. DNA was stained with Hoechst 33342. Scale bars, 50 μm. See also Figure S1 and Table S1.



(legend on next page)

marked increase of proliferation in intervillous domains compared with  $p57^{+/+}$  mice (Figures 1E and 1F). Normal proliferation levels in  $p57^{CK-}$  intestines indicate that the  $p57^{CK-}$  protein is still able to limit proliferation in the crypt and that increased proliferation in  $p57^{KO}$  is not due to loss of CDK inhibition by p57 (Figures 1E and 1F). These results were confirmed by labeling proliferating cells with proliferating cell nuclear antigen (PCNA) (Figure S1B). As previously reported,<sup>10</sup> p57 expression was only observed in villi and not at the bottom of crypts, where CBCs reside, and  $p57^{CK-}$  had a similar expression pattern (Figures 1G and S1B). The tissue alterations and increased proliferation observed in  $p57^{KO}$  mice may result from an expansion of the stem cell compartment. To test this hypothesis, ISC populations were monitored using reporter mice to genetically label these cells.

### p57 loss does not affect Lgr5<sup>+</sup> ISCs

To label Lgr5<sup>+</sup> ISCs,  $p57^{KO}$  and  $p57^{CK-}$  mice were intercrossed with Lgr5-eGFP-IRES-CreERT2 reporter mice (referred to as  $p57^{+/+};Lgr5^{+/eGFP-CreERT2}$ ,  $p57^{KO};Lgr5^{+/eGFP-CreERT2}$ , and  $p57^{CK-};Lgr5^{+/eGFP-CreERT2}$ ), in which GFP expression is driven by the Lgr5 promoter, allowing detection of CBCs with GFP.<sup>15</sup> Evaluation of Lgr5<sup>+</sup> ISC number by monitoring GFP on intestine cryosections did not reveal any significant difference between  $p57^{+/+}$ ,  $p57^{CK-}$ , and  $p57^{KO}$  embryos (Figures 2A and 2B). By flow cytometry, this mouse model allows visualizing a GFP<sup>High</sup> population that corresponds to CBCs and a GFP<sup>Low</sup> population corresponding to their immediate progeny, the TA cells.<sup>33</sup> Consistent with the histological data, the percentage of GFP<sup>High</sup> cells was not affected by p57 status ( $p57^{+/+}$ , 0.15% ± 0.02%;  $p57^{KO}$ , 0.17% ± 0.04%;  $p57^{CK-}$ , 0.14% ± 0.01%) (Figures 2C and 2D). On the other hand, the number of TA cells (GFP<sup>Low</sup>) was increased in  $p57^{KO}$  intestine (1.06% ± 0.18%) compared with  $p57^{+/+}$  (0.58% ± 0.05%) and  $p57^{CK-}$  (0.48% ± 0.13%) animals (Figures 2C and 2D). A caveat of using this Lgr5-eGFP-IRES-CreERT2 model is that transgene expression is known to be variegated, with approximately 25% of crypts expressing GFP,<sup>15,43</sup> which likely leads to an underestimation of the actual number of Lgr5<sup>+</sup> cells and could introduce some inter-individual variability. Nevertheless, all our analyses were performed in the same Lgr5-eGFP-IRES-CreERT2 genetic background and a high number of animals of each genotype was used to avoid a potential bias introduced by the variegation of the model. In addition, we obtained similar results when Lgr5<sup>+</sup> CBC numbers were evaluated by immunostaining for Olfm4

(Figures S2A and S2B), a known Lgr5<sup>+</sup> ISC marker.<sup>44</sup> These results were also confirmed using Id1 immunostaining, which labels both ISCs and TA cells.<sup>45</sup> In agreement with the flow cytometry data,  $p57^{KO}$  intestine exhibited more Id1<sup>+</sup> cells than  $p57^{+/+}$  and  $p57^{CK-}$  mice (Figures 2E and 2F). The identity and molecular signature of GFP<sup>High</sup>, GFP<sup>Low</sup>, and GFP<sup>Neg</sup> cells observed by flow cytometry was verified by RT-qPCR on sorted populations (Figures S2C–S2E). As expected, GFP<sup>High</sup> cells exhibited strong expression of CBC markers such as Lgr5, Ascl2, and Olfm4, and low expression of differentiation markers (Muc2, Muc4, and Sucrase) (Figures S2C and S2D). These cells also expressed moderate levels of reserve ISC markers such as mTert, Sox9, and, to a lower extent, of Hopx and Mex3a (Figure S2E), as previously described.<sup>33,34,36</sup> Taken together, our data indicate that p57 does not affect Lgr5<sup>+</sup> ISC abundance, consistent with p57 not being expressed in the lower crypt; however, p57 loss causes an increase in the number of progenitor cells in a CDK-independent manner.

### p57 deficiency leads to hyperproliferation of Hopx<sup>+</sup> ISCs

Hopx<sup>3xFLAG-eGFP</sup> reporter mice, in which Hopx is expressed as a FLAG-tagged eGFP fusion protein, were previously used successfully to label +4 reserve ISCs.<sup>29,35,46–49</sup> To label Hopx<sup>+</sup> ISCs,  $p57^{KO}$  and  $p57^{CK-}$  mutant mice were crossed with Hopx<sup>3xFLAG-eGFP</sup> reporter mice (referred to as  $p57^{+/+};Hopx^{+/3xFLAG-eGFP}$ ,  $p57^{KO};Hopx^{+/3xFLAG-eGFP}$  and  $p57^{CK-};Hopx^{+/3xFLAG-eGFP}$ ). Flow cytometry analyses in E18.5 intestines revealed a marked increase of the number of Hopx-GFP<sup>+</sup> cells in the absence of p57 (0.94% ± 0.09%) compared with  $p57^{+/+}$  (0.56% ± 0.03%) and  $p57^{CK-}$  (0.39% ± 0.02%) mice (Figures 3A and 3B). The molecular identity of Hopx-GFP<sup>+</sup> cells was verified by RT-qPCR after sorting. These cells exhibited increased expression of several +4 ISC markers described previously in the adult, including Hopx, Sox9, and Mex3a<sup>11,36</sup> (Figure S3A). A modest but consistent enrichment of the CBC markers Lgr5 and Ascl2 was also observed in these cells (Figure S3B), in agreement with previous reports.<sup>11,36,37</sup> Finally, Hopx-GFP<sup>+</sup> cells expressed significant amounts of Atoh1, consistent with the idea that reserve ISCs are in fact progenitors committed to the secretory lineage (Figure S3C).<sup>36</sup> Several studies reported that +4 ISCs are mostly quiescent or slowly cycling in homeostatic conditions, with only approximately 20% of cycling cells.<sup>25,27,29,49</sup> To determine if the increased number of Hopx-GFP<sup>+</sup> cells in  $p57^{KO}$  intestine is caused by a re-entry in the cell cycle, their proliferation was evaluated by

### Figure 2. Loss of p57 does not affect Lgr5<sup>+</sup> ISCs

- (A) Representative images of  $p57^{+/+};Lgr5^{+/eGFP-CreERT}$ ,  $p57^{KO};Lgr5^{+/eGFP-CreERT}$ , and  $p57^{CK-};Lgr5^{+/eGFP-CreERT}$  intestine sections at E18.5 immunostained for p57 (red), GFP (green), and E-cadherin (white). Scale bars, 50  $\mu$ m.
- (B) Number of Lgr5<sup>+</sup> (GFP<sup>+</sup>) cells by intervillous domain in  $p57^{+/+};Lgr5^{+/eGFP-CreERT}$  (n = 5),  $p57^{KO};Lgr5^{+/eGFP-CreERT}$  (n = 4), and  $p57^{CK-};Lgr5^{+/eGFP-CreERT}$  (n = 2) intestines counted from immunostained sections as described in (A). Graph shows means.
- (C) Representative dot plots of dissociated intestines from  $p57^{+/+};Lgr5^{+/+}$ ,  $p57^{+/+};Lgr5^{+/eGFP-CreERT}$ ,  $p57^{KO};Lgr5^{+/eGFP-CreERT}$ , or  $p57^{CK-};Lgr5^{+/eGFP-CreERT}$  E18.5 embryos analyzed by flow cytometry for GFP expression. Respective percentages of GFP<sup>High</sup> (CBCs, top) and GFP<sup>Low</sup> (TAs, bottom) are indicated for the individuals displayed.
- (D) Mean percentage of GFP<sup>High</sup> (CBCs, left panel) and GFP<sup>Low</sup> (TA cells, right panel) cells from flow cytometry analyses of  $p57^{+/+};Lgr5^{+/eGFP-CreERT}$  (n = 29),  $p57^{KO};Lgr5^{+/eGFP-CreERT}$  (n = 16), or  $p57^{CK-};Lgr5^{+/eGFP-CreERT}$  (n = 10) E18.5 intestines as described in (C). Graphs shows means ± SEM. One-way ANOVA; ns, p > 0.05; \*p ≤ 0.05; \*\*p ≤ 0.01.
- (E) Representative images of Id1 immunohistochemistry (brown) of intestine sections from  $p57^{+/+}$ ,  $p57^{KO}$ , and  $p57^{CK-}$  E18.5 embryos. Scale bars, 50  $\mu$ m.
- (F) Number of Id1<sup>+</sup> cells per intervillous domain in  $p57^{+/+}$  (n = 9),  $p57^{KO}$  (n = 6), and  $p57^{CK-}$  (n = 5) intestines as described in (E). Graph shows means ± SEM. One-way ANOVA; ns, p > 0.05; \*\*p ≤ 0.01; \*\*\*p ≤ 0.001. See also Figure S2.

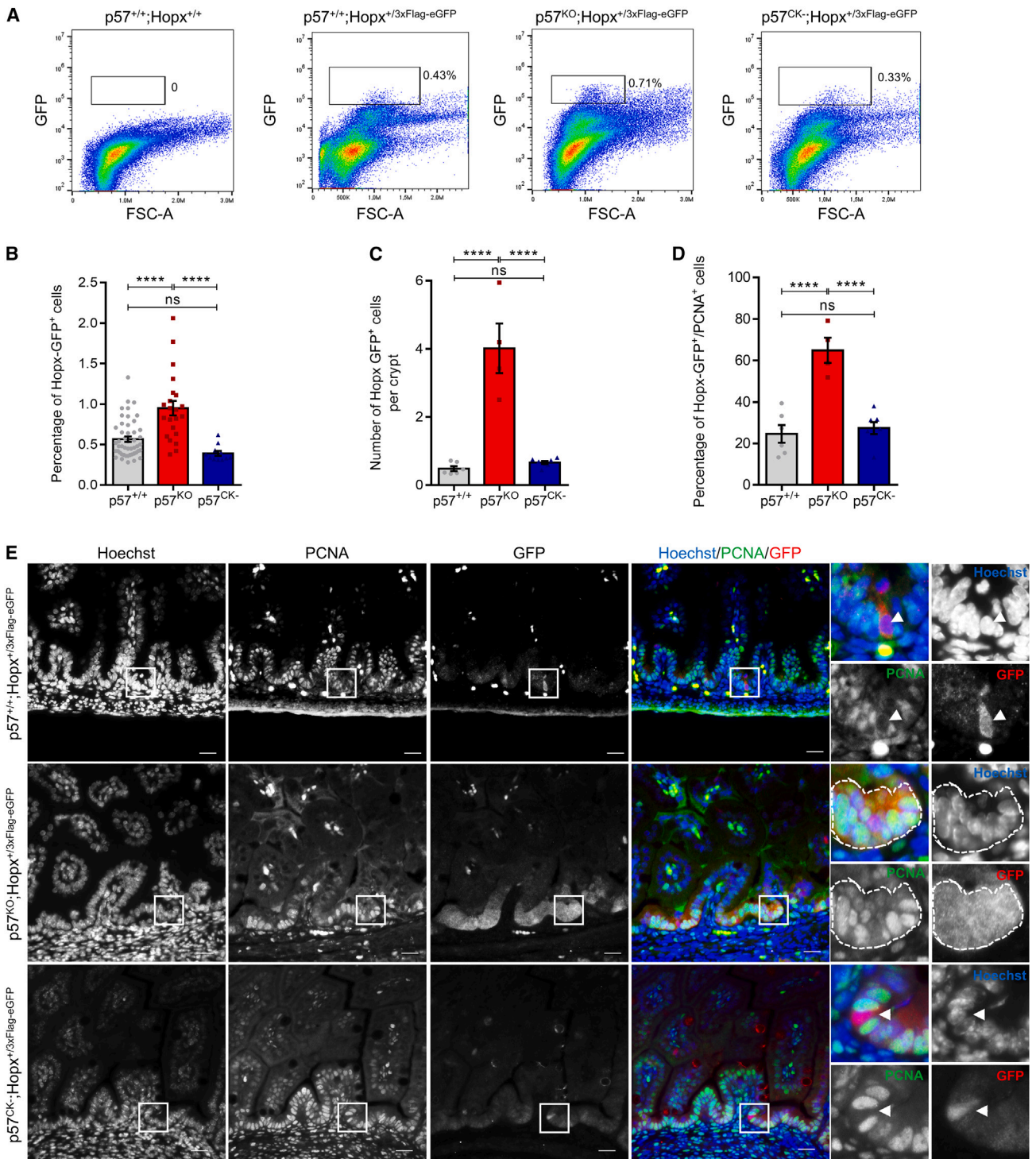


**Figure 3. Amplification and exit from quiescence of Hopx<sup>+</sup> ISCs in p57<sup>KO</sup> mice**

(A) Representative dot plots of dissociated intestines from p57<sup>+/+</sup>;Hopx<sup>+/+</sup>, p57<sup>+/+</sup>;Hopx<sup>+/3xFLAG-eGFP</sup>, p57<sup>KO</sup>;Hopx<sup>+/3xFLAG-eGFP</sup>, and p57<sup>CK-</sup>;Hopx<sup>+/3xFLAG-eGFP</sup> E18.5 embryos analyzed by flow cytometry for GFP expression. Respective percentages of GFP<sup>+</sup> cells are indicated for the individuals displayed.

(B) Mean percentage of Hopx-GFP<sup>+</sup> cells in flow cytometry analyses of p57<sup>+/+</sup>;Hopx<sup>+/3xFLAG-eGFP</sup> (n = 51), p57<sup>KO</sup>;Hopx<sup>+/3xFLAG-eGFP</sup> (n = 23), and p57<sup>CK-</sup>;Hopx<sup>+/3xFLAG-eGFP</sup> (n = 14) E18.5 intestines as described in (A). Graph shows means ± SEM. One-way ANOVA; ns, p > 0.05; \*\*\*\*p ≤ 0.0001.

(C) Mean number of Hopx-GFP<sup>+</sup> cells by intervillous domain in p57<sup>+/+</sup>;Hopx<sup>+/3xFLAG-eGFP</sup> (n = 6), p57<sup>KO</sup>;Hopx<sup>+/3xFLAG-eGFP</sup> (n = 4), and p57<sup>CK-</sup>;Hopx<sup>+/3xFLAG-eGFP</sup> (n = 7) E18.5 intestines immunostained for GFP and PCNA as shown in (E). Graph shows means ± SEM. One-way ANOVA; ns, p > 0.05; \*\*\*\*p ≤ 0.0001.

(legend continued on next page)

GFP/PCNA co-immunostaining (Figures 3C–3E). Consistent with the flow cytometry results, quantification of GFP<sup>+</sup> cells confirmed the increased number of Hopx-GFP<sup>+</sup> cells per intervillous domain in p57<sup>KO</sup> mice (Figure 3C). Moreover, there was a strong increase in the number of PCNA-positive Hopx-GFP<sup>+</sup> cells in p57<sup>KO</sup> (~65%) intestines, while it was approximately 25% in p57<sup>+/+</sup> and p57<sup>CK-</sup> intestines (Figures 3D and 3E).

Sox9 was described previously as an ISC marker, with Lgr5<sup>+</sup> ISCs being Sox9<sup>Low</sup> and reserve ISCs Sox9<sup>High</sup>.<sup>30,31,50</sup> To confirm our results, Sox9 immunostaining was used to monitor both ISC populations in function of p57 status (Figure S4). In agreement with the results obtained by genetic labeling of Hopx<sup>+</sup> and Lgr5<sup>+</sup> cells, the absence of p57 clearly increased the number of Sox9<sup>High</sup> cells but did not affect the number of Sox9<sup>Low</sup> cells (Figures S4A–S4C). In contrast, p57<sup>CK-</sup> mice had the same phenotype as p57<sup>+/+</sup> mice. Moreover, co-immunostaining for Sox9 and PCNA indicated that loss of p57 induces the proliferation of Sox9<sup>High</sup> cells, with ~65% of Sox9<sup>High</sup> cells co-expressing PCNA in p57<sup>KO</sup>, while only ~20% of Sox9<sup>High</sup> cells were PCNA positive in p57<sup>+/+</sup> and p57<sup>CK-</sup> intestines (Figures S4D and S4E), as reported previously,<sup>31,49</sup> confirming the results obtained using Hopx as a +4 ISC marker (Figures 3D and 3E). As described above, in the absence of p57, we also observe an increase of TA cells. Since Klf4 has been described to be highly expressed in some early-differentiated TA cells, we performed Klf4/p57 co-immunostaining in E18.5 intestines. Similarly to p57, Klf4 expression can be detected along the entire length of the mouse intestine, mainly in non-proliferating, terminally differentiated epithelial cells (Figure S5A, white arrowheads). A strong expression of Klf4 was also detected in goblet cells, easily distinguished by their morphology (Figure S5A, red arrowheads), consistent with Klf4 being strongly expressed in goblet cells in single-cell RNA sequencing (RNA-seq) signature<sup>51</sup> and with its role in their terminal differentiation.<sup>52,53</sup> On the other hand, p57 expression was not detected in goblet cells (Figure S5A). In the TA compartment, we did not observe a co-expression of Klf4 and p57 (Figure S5A). In the intervillous domain, p57 expression was detected in cells near/at the +4 position, while Klf4 was expressed in few cells scattered in the crypt area, most likely differentiated secretory cells such as goblet or Paneth cells (Figures S5B and S5C). Thus, these results support the fact that the increase of TA cells results from the expansion of Hopx<sup>+</sup> cells that re-enter the cell cycle, generating additional progenitors.

Overall, these results suggest that p57 plays a critical role in maintaining quiescence in +4 ISCs, independently of CDK inhibition.

### Loss of p57 causes major gene expression changes in Hopx<sup>+</sup> ISCs

The expression of p57 was evaluated by RT-qPCR in both ISC populations. Consistent with p57 immunostaining (Figure 1G

and S1B) showing no signal in lower crypts, p57 was expressed at low levels in Lgr5<sup>+</sup> ISCs (GFP<sup>High</sup>) and TA cells (GFP<sup>Low</sup>) but was abundant in differentiated (GFP<sup>Neg</sup>) cells (Figure 4A). In contrast, p57 mRNA expression was high in Hopx-GFP<sup>+</sup> cells (Figure 4B), in agreement with the reported expression of p57 in Mex3a<sup>High</sup> or Bmi1<sup>High</sup> ISCs.<sup>11,12</sup> To confirm the expression of p57 in Hopx<sup>+</sup> cells, p57 expression was investigated by immunostaining of E18.5 intestines from p57<sup>+/+</sup>;Hopx<sup>+/3xFLAG-eGFP</sup>. In keeping with RT-qPCR results, p57 expression was detected in Hopx-GFP<sup>+</sup> cells localized around the +4 position (Figures S6A and S6B). Interestingly, cytoplasmic localization of p57 was observed in some, but not all, Hopx-GFP<sup>+</sup> cells (Figure S6B), suggesting an active regulation of p57 shuttling in these cells.

To further define the role of p57 in Hopx<sup>+</sup> cells, RNA-seq analyses were performed on Hopx-GFP<sup>+</sup> cells sorted from p57<sup>+/+</sup> or p57<sup>KO</sup> E18.5 intestines to compare their bulk RNA profiles. In the entire genome, 21,110 genes were expressed at appreciable level (>50 reads per kilobase per million mapped reads [RPKM] in total on the 10 samples). Differential DESeq2 analysis revealed that 6,111 genes were deregulated in p57<sup>KO</sup> mice ( $p < 0.05$  and absolute log<sub>2</sub> fold change >1), with 3,129 genes upregulated and 2,982 downregulated (Figures 4C and 4D; Table S2). We next investigated how p57 status affected the gene expression signature of different intestinal cell populations previously published.<sup>11,51</sup> Strikingly, loss of p57 resulted in increased expression of genes found in the signature of CBCs and TA cells (Figures 4E and 4F), supporting the idea that p57<sup>KO</sup> Hopx<sup>+</sup> cells exit quiescence and behave like proliferative ISCs. For instance, expression of Lgr5, Ascl2, Olfm4, and Id1 approximately doubled in p57<sup>KO</sup> Hopx<sup>+</sup> cells compared with p57<sup>+/+</sup> (mean fragments per kilobase of exon per million mapped fragments [FPKM] 5.07 vs. 2.62, 3.87 vs. 1.95, 102.6 vs. 57.42, and 61.53 vs. 26.2, respectively). The signature genes of LRCs and Mex3a<sup>High</sup> cells were also expressed at higher levels in p57<sup>KO</sup> Hopx<sup>+</sup> ISCs (Figures 4G and 4H). Interestingly, p57<sup>KO</sup> Hopx<sup>+</sup> cells also expressed higher levels of genes present in differentiated intestinal epithelial cells of both secretory (enteroendocrine and goblet) and absorptive (enterocytes) lineages (Figures S6C–S6E). This likely reflects the increased number of committed progenitors (TA cells) in the absence of p57 and indicates that Hopx<sup>+</sup> cells are capable of generating both secretory and absorptive progenies. Taken together, these results indicate that, in the absence of p57, quiescent Hopx<sup>+</sup> cells become proliferative and acquire markers of proliferative Lgr5<sup>+</sup> ISCs, as well as of committed progenitor cells.

### p57 interacts with Ascl2 and inhibits its transcriptional activity

In neural progenitors, p57 was reported to promote their maintenance and prevent differentiation by binding to and inhibiting the transcription factor Ascl1.<sup>54</sup> Ascl2, a paralog of Ascl1, is also a

(D) Mean percentage of proliferative Hopx-GFP<sup>+</sup> ISCs, positive for both GFP and PCNA, in intestines as described in (C). Graph shows means ± SEM. One-way ANOVA; ns,  $p > 0.05$ ; \*\*\*\* $p \leq 0.0001$ .

(E) Representative images of GFP and PCNA immunostaining of p57<sup>+/+</sup>;Hopx<sup>+/3xFLAG-eGFP</sup>, p57<sup>KO</sup>;Hopx<sup>+/3xFLAG-eGFP</sup>, and p57<sup>CK-</sup>;Hopx<sup>+/3xFLAG-eGFP</sup> E18.5 intestines. Arrowheads or the dashed line point to the GFP<sup>+</sup> cells in the enlarged areas. DNA was stained with Hoechst 33342. Scale bars, 20 μm. See also Figures S3 and S4.

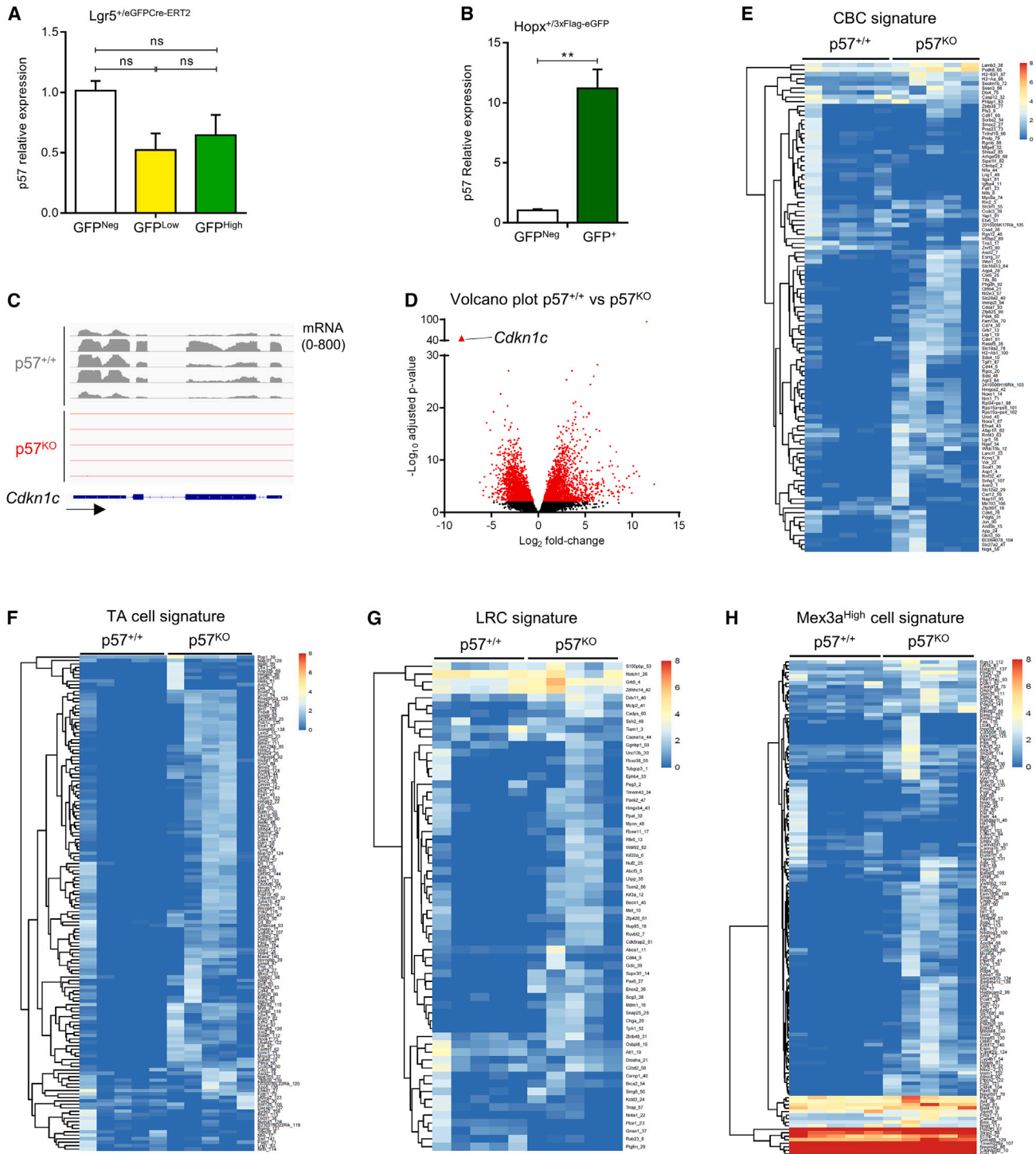


**Figure 4. Transcriptomic analyses show major gene expression changes in Hopx<sup>+</sup> ISCs of p57<sup>KO</sup> mice**

(A and B) p57 is expressed in Hopx<sup>+</sup> stem cells. Relative p57 expression levels, evaluated by RT-qPCR, in cells sorted based on GFP expression from dissociated crypts from *Lgr5<sup>+</sup>eGFP-CreERT2* (A) and *Hopx<sup>+</sup>3xFLAG-eGFP* (B) intestines. p57 mRNA levels were normalized to GAPDH expression and expressed relative to expression in GFP<sup>Neg</sup> cells. Graphs show means ± SEM. Data were compared using one-way ANOVA (A) ns,  $p > 0.05$  or unpaired two-tailed Student's *t* test (B) \*\* $p \leq 0.01$ .

(C–H) Hopx-GFP<sup>+</sup> cells were sorted from dissociated crypts from E18.5 p57<sup>+/+</sup> ( $n = 5$ ) and p57<sup>KO</sup> ( $n = 5$ ) embryos and submitted to RNA-seq analysis.

(C) Genome Browser image capture for RNA-seq coverage of p57 mRNA ( $|\log_2FC| = -8.7$ ; adjusted  $p = 3.9e^{-47}$ ).

(legend continued on next page)

basic-helix-loop-helix transcription factor that activates transcription by binding DNA on E-box motifs (CANNTG).<sup>41</sup> Ascl2 plays a key role in Lgr5<sup>+</sup> ISC specification and maintenance, and its re-expression and activation are required for Lgr5<sup>+</sup> ISC regeneration following crypt damage.<sup>40,42</sup> Ascl2 acts synergistically with Wnt signaling to control the expression of key ISC genes, including Lgr5, Sox9, and EphB3.<sup>41</sup> Here, we tested whether p57 inhibits Ascl2 activity to regulate ISC fate and proliferation.

An interaction between p57 and Ascl2 was shown by co-immunoprecipitation (coIP) in HEK293 cells (Figures 5A and 5B). This interaction was also detected between p57<sup>CK-</sup> and Ascl2, indicating that the interaction does not require cyclin-CDK complexes; however, in these experiments, p57<sup>CK-</sup> binding to Ascl2 was consistently lower than with wild-type p57, suggesting that the point mutations in the cyclin and/or CDK-binding domains of p57<sup>CK-</sup> affect this interaction (Figures 5A and 5B). Indeed, the interaction of p57 with other transcription factors, such as MyoD or b-Myb, was previously reported to take place within the cyclin-CDK-binding region of p57.<sup>55-57</sup> The p57/Ascl2 interaction was confirmed by proximity ligation assays (PLAs) on endogenous proteins in SW480 cells (Figure 5C). The effect of p57 on Ascl2 transcriptional activity was determined in transcription reporter assays in which a destabilized GFP (half-life ~ 1 h) under the control of the Sox9 or Lgr5 promoter (Figure 5D) was co-transfected in HEK293 cells with Ascl2 and increasing amounts of p57 or p57<sup>CK-</sup>. Results were normalized to the activity of the GAPDH promoter obtained in the same conditions. Transfection of increasing amounts of p57 decreased Sox9 and Lgr5 promoter activity, indicating a significant inhibition of Ascl2 transcriptional activity, while no statistically significant effect was observed when the Phox2A promoter, an Ascl1 target,<sup>54</sup> was used (Figure 5E). Similar results were obtained when p57<sup>CK-</sup> was expressed (Figure 5F), indicating that repression of Ascl2 activity is a CDK-independent process. Finally, monitoring of the expression of 21 known Ascl2 target genes<sup>42</sup> in the RNA-seq from sorted Hopx-GFP<sup>+</sup> cells indicated that 11 of them were significantly upregulated in p57<sup>KO</sup> compared with p57<sup>+/+</sup> Hopx<sup>+</sup> cells (Figure 5G), confirming the idea that p57 acts as a transcriptional repressor toward Ascl2. Thus, these data indicate that p57 can bind to and inhibit Ascl2 transcriptional activity in a CDK-independent manner.

### p57 participates in the recruitment of a corepressor complex to Ascl2 target gene promoters

We previously identified HDAC7 as a potential p57-binding partner in the p57 interactome.<sup>5</sup> HDAC7 is a class II HDAC that represses transcription via the formation of a repressor complex, notably with the scaffold protein mSin3a.<sup>58</sup> Interactions between p57 or p57<sup>CK-</sup> and HDAC7 (Figure 6A) or mSin3a (Figure 6B) were detected by coIP in HEK293 cells. Again, p57<sup>CK-</sup> appeared to interact more weakly with these partners than wild-type p57,

especially with mSin3a, indicating that (1) p57 binding to these partners is independent of cyclin/CDK complexes, and (2) the N-terminal cyclin/CDK-binding region may be involved in these interactions. The formation of a protein complex between p57, HDAC7, and mSin3a was validated by coIP on endogenous proteins in SW480 cells (Figures 6C and 6D), and these interactions were confirmed by PLA experiments as well (Figure 6E). Similarly, coIP experiments revealed that Ascl2 also binds to HDAC7 and mSin3a in HEK293 cells overexpressing these proteins (Figure S7A), and these interactions were confirmed by PLA on endogenous proteins in SW480 cells (Figure S7B).

Finally, the presence of p57 and the corepressor complex subunits on Ascl2 target gene promoters was investigated by chromatin immunoprecipitation (ChIP) in SW480 cells. As expected, Ascl2 was present on the promoters of Lgr5, Sox9, and EphB3 (Figures 7A and S8A),<sup>42</sup> and p57, HDAC7, and mSin3a were also detected on the same sequences of these Ascl2 target promoters (Figures 7B–7D and S8B–S8D). To confirm that p57 is recruited to DNA by Ascl2, pull-down assays using streptavidin beads bound to biotinylated oligonucleotides containing the E-box of the Lgr5 promoter or a control oligonucleotide with point mutations in the E-box were performed on HEK293 cells transfected with Ascl2 and/or p57 (Figure 7E) or p57<sup>CK-</sup> (Figure 7F). p57 and p57<sup>CK-</sup> required DNA-bound Ascl2 and a functional E-box to bind the beads (Figures 7E and 7F). Similar experiments with cells also expressing HDAC7 or mSin3a indicated that these corepressor proteins bound to the E-box-containing oligonucleotide but not to the E-box mutant oligonucleotide (Figures 7G and 7H).

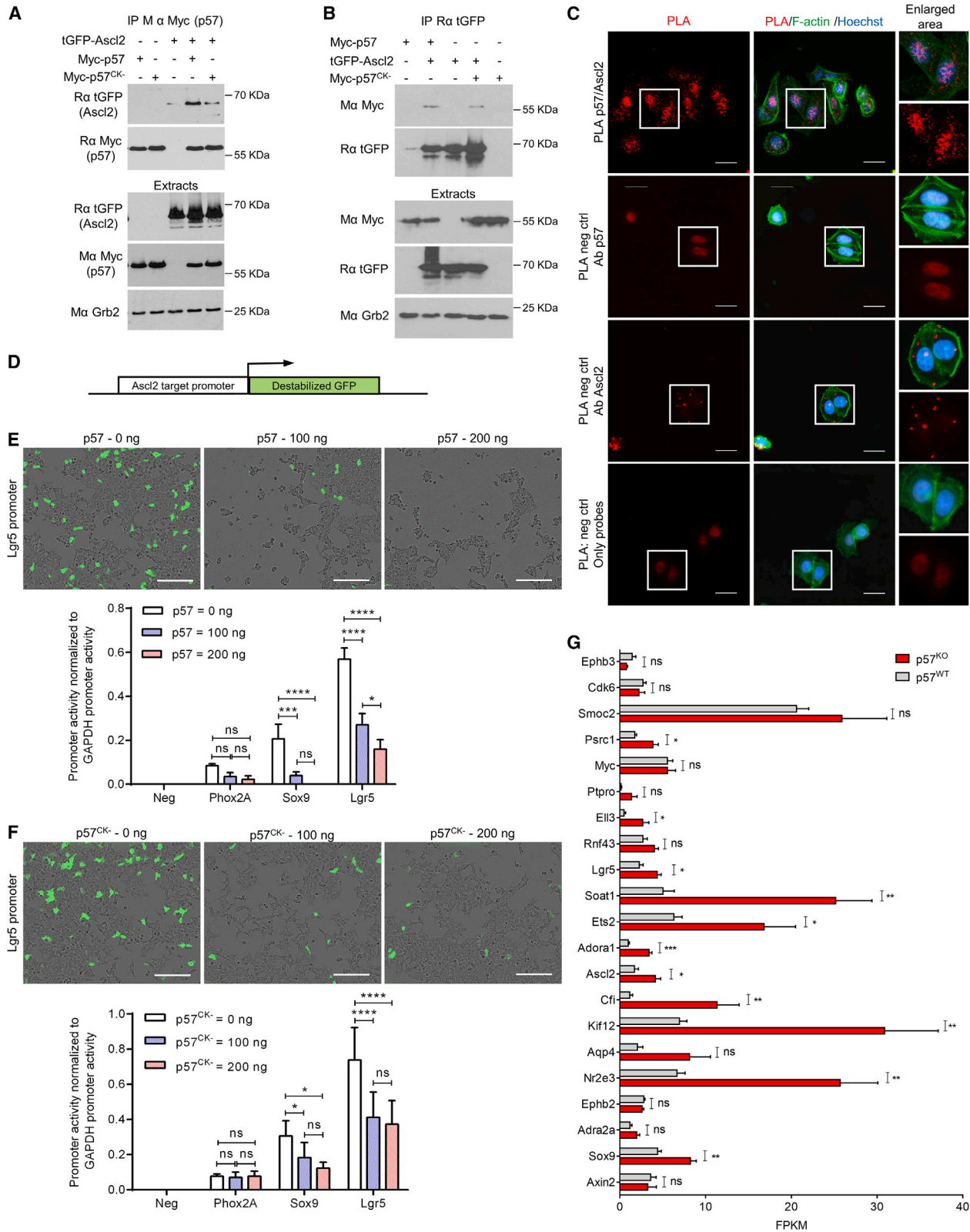
To determine whether p57 mediates the recruitment of the corepressor complex proteins to Ascl2 target genes, ChIPs were performed after p57 silencing with small interfering RNAs (siRNAs) (Figure 7I). The knockdown of p57 markedly decreased the amount of HDAC7 present on Ascl2 target gene promoters in SW480 cells (Figures 7J and S8E). Consistent with the idea that p57 participates in the recruitment of a corepressor complex with histone deacetylase activity to Ascl2 target gene promoters, increased histone H3 lysine acetylation (H3K27-Ac) was observed at these promoters when p57 expression was silenced, suggesting a derepression of chromatin (Figures 7K and S8F). Overall, these results suggest that p57 is able to inhibit Ascl2 transcriptional activity by participating in the recruitment of a corepressor complex containing HDAC7 and mSin3a to Ascl2 target gene promoters, thereby regulating ISC fate and proliferation.

### DISCUSSION

The entire intestinal epithelium is renewed every few days by Lgr5<sup>+</sup> ISCs residing at the bottom of the crypts.<sup>15</sup> In case of genotoxic or cytotoxic damage, Lgr5<sup>+</sup> ISCs are lost and must be rapidly regenerated to maintain epithelial integrity.<sup>14</sup> Whether Lgr5<sup>+</sup> ISCs are regenerated by dedifferentiation of committed progenitors that re-enter the niche or by dedicated

(D) Volcano plot for mRNA expression changes in p57<sup>+/+</sup> vs. p57<sup>KO</sup> Hopx-GFP<sup>+</sup> cells as described above. Differential gene expression in function of p57 status was determined by DEseq2 analysis of RNA-seq. Red dots represent significantly deregulated genes ( $|\log_2FC| > 1$  and adjusted p value < 0.05).

(E–H) Heatmaps of Hopx-GFP<sup>+</sup> ISC RNA-seq FPKM from p57<sup>+/+</sup> (n = 5) and p57<sup>KO</sup> (n = 5) mice for previously published gene expression signatures of specific intestinal cell populations: CBCs (E) TA cells (F), LRCs (G), and Mex3a<sup>High</sup> cells (H). See also Figure S6.



(legend on next page)

reserve stem cells that are normally quiescent is still debated<sup>22,23,25,29,32,36,40,50,59</sup> (see section “limitations of the study” below).

We found that, during late development, loss of p57 expression triggers an expansion of the dividing compartment in intestinal crypts, with an amplification of TA cells and of a Hopx<sup>+</sup> cell population previously described as reserve ISCs in adult mice,<sup>46</sup> while the number of Lgr5<sup>+</sup> ISCs was not affected. In the absence of p57, Hopx<sup>+</sup> ISCs become proliferative instead of being mostly quiescent, and cell cycle re-entry is associated with a derepression of Ascl2 activity and increased expression of its target genes. This is consistent with a recent report showing that Ascl2 re-expression in committed progenitors is required for Lgr5<sup>+</sup> ISC regeneration after damage.<sup>40</sup> Thus, during intestinal development, p57 appears to limit the stem cell niche and suppress the proliferative ISC phenotype by repressing Ascl2 activity in Hopx<sup>+</sup> cells that are located just above the niche. Similarly, a recent study reported that, in adult mice, p57 is specifically expressed in Bmi1<sup>+</sup> reserve ISCs and is involved in maintaining their quiescence, although the mechanism involved was not investigated.<sup>12</sup>

RNA-seq analyses of sorted Hopx<sup>+</sup> cells from E18.5 intestines show that p57 loss shifts their gene expression signature toward that of CBCs and a number of cell cycle regulatory genes, including cyclins A2, B1, B2, CDK4, Cdc25a, and Cdc20, which are upregulated, consistent with re-entry in the cell cycle. In addition, differentiation markers for all intestinal cell types are also present in this sorted cell population, suggesting that these Hopx<sup>+</sup> cells are indeed *bona fide* ISCs capable of giving rise to progenitors committed toward all intestinal lineages. Importantly, intestine development and ISC populations were normal in p57<sup>CK−</sup> mice, indicating that p57-mediated cyclin-CDK inhibition is not essential to maintain intestinal epithelium homeostasis and quiescence outside of the crypt. Quiescence of differentiated cells is probably enforced by other CKIs such as p27, which has a similar expression pattern to p57 in the intestine.<sup>10</sup> In Hopx<sup>+</sup> cells, our data suggest that p57 maintains quiescence by inhibiting the transcriptional activity of Ascl2, thereby repressing the Lgr5<sup>+</sup> ISC phenotype.

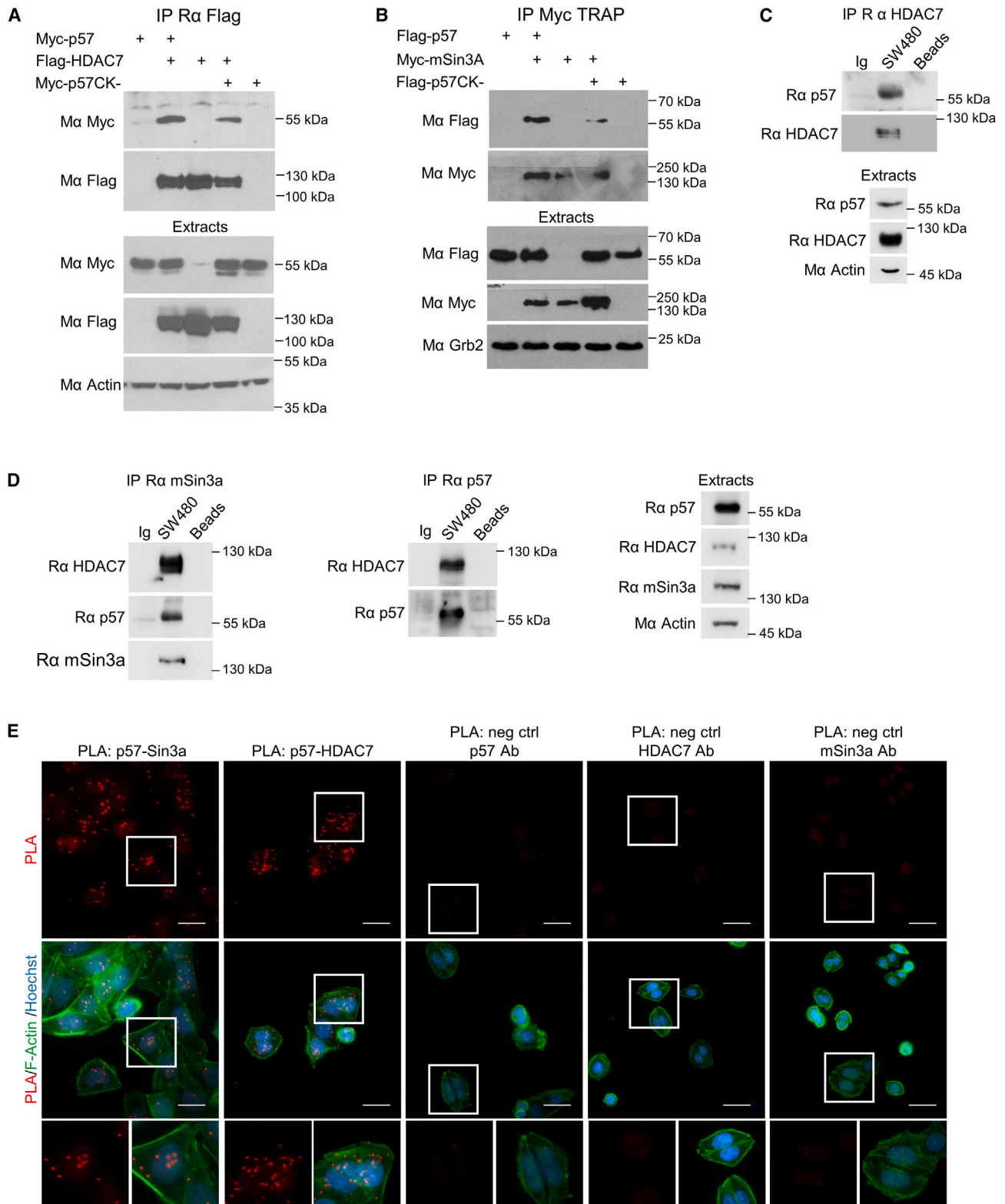
Several studies have described the ability of p57 to regulate transcription by distinct mechanisms. For instance, p57 binds to and promotes MyoD activity by preventing CDK-mediated phosphorylation and targeting of MyoD for degradation, as

well as by another unknown mechanism independent of CDKs.<sup>55</sup> Conversely, p57 was found to bind to and inhibit the transcriptional activity of Ascl1 independently of CDKs, although the underlying mechanism was not investigated.<sup>54</sup> p57 may also control transcription by regulating RNA polymerase II C-terminal domain (CTD) phosphorylation in an E2F1-dependent manner.<sup>60</sup> More recently, p57 was found to promote c-Jun and FHL2-mediated transcription by competing with HDAC1 and HDAC3 for binding to these transcription factors, thereby relieving their inhibition by HDACs.<sup>61,62</sup> Interestingly, while the N terminus of p57 acted as a transactivator, presumably by competing with HDACs, the C terminus of p57 repressed c-Jun activity, suggesting a complex regulation that may depend on the binding partners and/or on posttranslational modifications of p57.<sup>61</sup> Herein, we found that p57 could interact with HDAC7 and with the corepressor mSin3a in a CDK-independent manner, suggesting that p57 may function as a transcriptional corepressor by recruiting a repressor complex to specific promoters, in a manner similar to p27.<sup>63</sup> In agreement with this idea, p57 is present on chromatin at Ascl2 target promoters and appears to control the recruitment of these corepressors to promoters. Indeed, p57 knockdown resulted in decreased presence of HDAC7 on Ascl2 target gene promoters, as well as in increased histone H3 acetylation levels, which is consistent with derepression of these promoters, a possibility that was confirmed by RNA-seq analyses.

Interestingly, two transcriptional corepressors, RUNX1T1 (MTG8) and CBFA2T3 (MTG16), were recently found to be expressed in cells at the +4/+5 positions and to control the fate of these progenitors/stem cells, directing them toward differentiation in the enterocyte lineage.<sup>64</sup> *Runx1t1* knockout and *Runx1t1/Cbfa2t3* double-knockout mice die shortly after birth and exhibit intestinal shortening.<sup>64</sup> This was accompanied by increased proliferation in the crypts and increased expression of Lgr5<sup>+</sup> ISC signature genes.<sup>64</sup> RUNX1T1 and CBFA3T2 act as transcriptional corepressors by binding to mSin3a, several HDACs, and the nuclear receptor corepressor (N-CoR) and silencing mediator of retinoic acid and thyroid hormone receptor (SMRT) complexes.<sup>65</sup> Given the phenotypic similarities of the *Runx1t1* and *Runx1t1/Cbfa2t3* knockout mice to those of p57<sup>KO</sup> mice, it would be interesting to test if RUNX1T1 and/or CBFA2T3 are present in the corepressor complex in which p57 is involved.

### Figure 5. p57 binds to and inhibits Ascl2

- (A) p57 or p57<sup>CK−</sup> was immunoprecipitated with Myc antibodies from HEK293 cells transfected with tGFP-Ascl2 and/or Myc-p57 or Myc-p57<sup>CK−</sup> and the presence of Ascl2 was assessed by immunoblotting (n = 3). Amounts of transfected proteins in lysates are shown. Grb2 was used as loading control.
- (B) Ascl2 was immunoprecipitated with turbo-GFP (tGFP) antibodies from HEK293 cells transfected with tGFP-Ascl2 and/or Myc-p57 or Myc-p57<sup>CK−</sup> and the presence of p57 was determined by immunoblot (n = 3). Amounts of transfected proteins in lysates are shown. Grb2 was used as loading control.
- (C) PLA using p57 and Ascl2 antibodies on endogenous proteins in SW480 cells. F-actin was stained with phalloidin and DNA with Hoechst 33342. Scale bars, 50 μm. Representative images from three independent experiments.
- (D) Schematic of a pZsGreen reporter construct in which a destabilized GFP (half-life ~ 1 h) is cloned downstream of a promoter to measure promoter activity.
- (E and F) HEK293 cells were co-transfected with 100 ng of a reporter construct [pZsGreen DA [no promoter, negative control], or pZsGreen pGAPDH [positive control], or pZsGreen pPhox2a [Ascl1 target], or pZsGreen pSox9, or pZsGreen pLgr5 [Ascl2 targets]], 100 ng of an Ascl2 expression vector, and the indicated amounts of a p57 (E) or p57<sup>CK−</sup> (F) expression vector. The number of fluorescent cells was quantified using an Incucyte FLR. Scale bars, 200 μm. Graphs represent the mean fluorescent object density normalized to that of GAPDH in the same condition from four independent experiments. Graphs show means ± SEM. Two-way ANOVA; ns, p > 0.05; \*p ≤ 0.05; \*\*p ≤ 0.001; \*\*\*\*p ≤ 0.0001.
- (G) Expression levels FPKM of Ascl2 target genes from van der Flier et al.<sup>42</sup> in RNA-seq data from p57<sup>+/+</sup> and p57<sup>KO</sup> Hopx-GFP<sup>+</sup> ISCs from Figure 4. Graphs show means ± SEM. Multiple unpaired two-tailed Student's t test; ns, p > 0.05; \*p ≤ 0.05; \*\*p ≤ 0.001.



(legend on next page)

The chromatin state of Lgr5<sup>+</sup> ISCs and committed progenitors are very similar, although the promoters/enhancers of lineage-restricted genes are selectively open in the latter, which may be reversed during their dedifferentiation into Lgr5<sup>+</sup> ISCs.<sup>66–68</sup> This suggests that the cellular plasticity in the intestinal epithelium and interconversion of ISCs does not require broad modifications of the chromatin state but may be mediated by modulating the activity of specific transcription factors, such as Ascl2, and/or by epigenetic modifications of a limited number of *cis*-acting elements.<sup>40,67</sup> Our data suggest that p57 acts as a key regulator of Ascl2 activity and participates in modulating the permissive state of chromatin at Ascl2-responsive promoters/enhancers. Thus, controlling p57 levels along the crypt-villus axis may constitute a powerful means to regulate cell fate in the intestinal epithelium.

Ascl2 is a target of the Wnt/LEF1/β-catenin pathway, whose expression is frequently upregulated in colorectal cancers.<sup>42,69,70</sup> Ascl2 was also involved in treatment resistance in colorectal cancer cells.<sup>71</sup> Conversely, *CDKN1C* is a putative tumor-suppressor gene, and epigenetic silencing of p57 is observed in colorectal cancers, correlating with poor prognosis.<sup>72–75</sup> Moreover, a recent study highlights the role of p57 in maintaining quiescence of colorectal cancer stem cells, conferring resistance to chemotherapeutic agents to these cells.<sup>76</sup> Our results could provide the molecular basis explaining the possible tumor-suppressor role of p57 in colorectal cancer. Indeed, p57 silencing may contribute to the derepression of Ascl2 activity in colorectal cancer cells and the acquisition of cancer stem cell characteristics.

Overall, our data suggests that p57 regulates intestinal development by maintaining quiescence of Hopx<sup>+</sup> ISCs in a CDK-independent manner, by repressing the transcriptional activity of Ascl2 via the recruitment of a corepressor complex. Thus, p57 appears to be a key regulator participating in the control of ISC fate and proliferation.

### Limitations of the study

As aforementioned, the precise identity of +4 reserve ISCs remains elusive as multiple markers have been described for these cells and it remains unclear whether they represent a single or distinct cell populations. Indeed, various markers, such as Bmi1,<sup>12,25,26</sup> mTert,<sup>28</sup> Hopx,<sup>29,35,47–49</sup> or Clusterin,<sup>32</sup> have been used to demonstrate the existence of a mostly quiescent cell population located at/near the +4 position that possesses ISC capacities that can be activated in a regeneration context following various types of injury. In addition, other studies reported the existence of subpopulation(s) of Lgr5<sup>+</sup> cells existing in a slow-cycling state, using the marker Mex3a<sup>High</sup><sup>11</sup> or their

ability to retain DNA label,<sup>36</sup> that can re-enter proliferation in case of intestinal damage. These cells exhibit similar gene expression signatures, indicating that they probably are secretory progenitors that can dedifferentiate to acquire ISC activity after injury.<sup>11,36</sup> In agreement with this secretory lineage signature, several studies have shown the capacity of secretory progenitors to dedifferentiate and act as stem cells.<sup>59,67,77</sup> Despite the controversy about their identity, all the populations described share important features, including their localization around the +4 position, their mostly quiescent state, their resistance to DNA damage, and their ability to act as ISCs and regenerate the intestinal epithelium after damage. Overall, an attractive and unifying theory is that +4 stem cells are a slow-cycling subpopulation of ISCs committed to the secretory lineage and able to re-enter proliferation in case of damage. However, a recent study challenged the quiescent reserve stem cell concept by showing that an actively cycling Msi1<sup>+</sup> population is in fact DNA damage resistant and supports intestinal epithelium regeneration,<sup>78</sup> reopening the questions of quiescence of reserve ISCs and of the genetic marker used.

While our data clearly show that, in p57<sup>CK−</sup> mice, the p57<sup>CK−</sup> protein can still restrain proliferation outside the crypts, implying that quiescence is maintained in a CDK-independent manner, the exact mechanism by which p57 maintains quiescence is not fully established. Indeed, we have not been able to clearly demonstrate that the increased proliferation observed in the crypts of p57<sup>KO</sup> intestines is caused by the derepression of Ascl2 activity. For instance, it could result from the loss of regulation of other transcription factors or signaling pathways regulated by p57.

### STAR★METHODS

Detailed methods are provided in the online version of this paper and include the following:

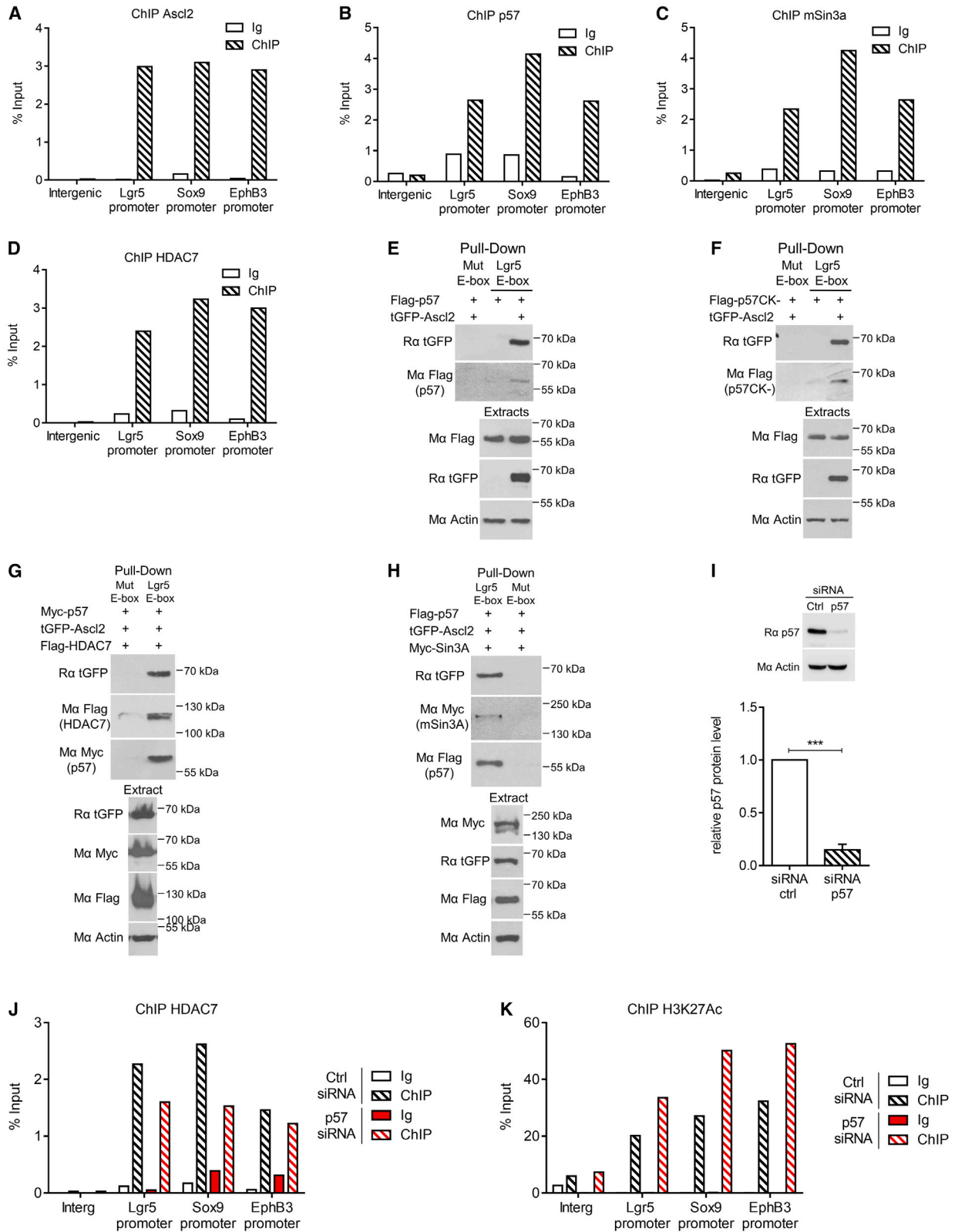
- KEY RESOURCES TABLE
- RESOURCE AVAILABILITY
  - Lead contact
  - Materials availability
- EXPERIMENTAL MODEL AND SUBJECT DETAILS
  - Mouse models
  - Cell culture and transfection
- METHOD DETAILS
  - Histology
  - Flow cytometry
  - Cell sorting
  - Reverse transcriptase and qPCR

### Figure 6. p57 forms a corepressor complex with HDAC7 and mSin3a

(A and B) HDAC7 (A) or mSin3a (B) were immunoprecipitated from HEK293 cells transfected with FLAG-HDAC7 or Myc-mSin3a and/or FLAG-p57 and/or FLAG-p57<sup>CK−</sup> and the presence of p57 was assessed by immunoblotting (n = 3). Amounts of transfected proteins in lysates are shown. Actin (A) or Grb2 (B) were used as loading control.

(C and D) Endogenous HDAC7 (C), mSin3a and p57 (D) were immunoprecipitated from SW480 cell lysates and the presence of endogenous p57, HDAC7, and/or mSin3a was assessed by immunoblotting. Protein A beads alone and control immunoglobulin G (IgG) were used as negative control. Respective levels of each protein in lysates are shown. β-Actin was used as loading control (n = 3).

(E) PLA for p57/mSin3a proximity and p57/HDAC7 proximity in SW480 cells using p57, mSin3a, and/or HDAC7 antibodies. F-actin was stained with phalloidin and DNA with Hoechst 33342. Scale bars, 50 μm. Representative images of three independent experiments. See also Figure S7.



(legend on next page)

- Co-immunoprecipitation
- DNA pull-down assays
- Immunoblotting
- GFP transcription reporter assays
- Chromatin immunoprecipitation
- Proximity Ligation Assay
- **QUANTIFICATION AND STATISTICAL ANALYSIS**
- Data and code availability

#### SUPPLEMENTAL INFORMATION

Supplemental information can be found online at <https://doi.org/10.1016/j.celrep.2023.112659>.

#### ACKNOWLEDGMENTS

We thank Dr Philippe Jay and Julie Nguyen (IGF, Montpellier, France) for expert advice on FACS of ISCs, Dr Ludivine Drougat (CBI, Toulouse, France) for useful discussion for RNA-seq data analysis and interpretation, and Dr Fabrice Escaffit (CBI, Toulouse, France) for advice on RT-qPCR. We are grateful to Dr. Eric Verdin (UCSF, San Francisco, CA) and Dr. Robert Eisenman (Fred Hutchinson Cancer Research Center, Seattle, WA) for providing reagents. The authors thank the personnel of the ABC animal facility. This work was supported by funds from the Fondation ARC pour la Recherche sur le Cancer, the Fondation Toulouse Cancer Santé, the Institut National Du Cancer (INCa\_14854), and an FRM Equipes grant (EQU202103012639) from the Fondation pour la Recherche Médicale.

#### AUTHOR CONTRIBUTIONS

J.C., A.N., A. Prel, M.A., N.D., T.J., C.D., and A.B. designed the experiments. J.C., A.N., A. Prel, A. Pizzoccaro, N.D., C.C., and A.B. performed the experiments. J.C., A.N., M.A., A. Prel, A. Pizzoccaro, N.D., and A.B. analyzed the data. J.C. and A.B. wrote the paper with contributions from all authors. A.B. acquired the funds and supervised the work.

#### DECLARATION OF INTERESTS

The authors declare no competing interests.

Received: September 19, 2022

Revised: December 1, 2022

Accepted: June 1, 2023

#### REFERENCES

1. Besson, A., Dowdy, S.F., and Roberts, J.M. (2008). CDK inhibitors: cell cycle regulators and beyond. *Dev. Cell* *14*, 159–169. <https://doi.org/10.1016/j.devcel.2008.01.013>.
2. Creff, J., and Besson, A. (2020). Functional versatility of the CDK inhibitor p57(Kip2). *Front. Cell Dev. Biol.* *8*, 584590. <https://doi.org/10.3389/fcell.2020.584590>.
3. Yan, Y., Frisé, J., Lee, M.H., Massagué, J., and Barbacid, M. (1997). Ablation of the CDK inhibitor p57Kip2 results in increased apoptosis and delayed differentiation during mouse development. *Genes Dev.* *11*, 973–983.
4. Zhang, P., Liégeois, N.J., Wong, C., Finegold, M., Hou, H., Thompson, J.C., Silverman, A., Harper, J.W., DePinho, R.A., and Elledge, S.J. (1997). Altered cell differentiation and proliferation in mice lacking p57KIP2 indicates a role in Beckwith-Wiedemann syndrome. *Nature* *387*, 151–158.
5. Duquesnes, N., Callot, C., Jeannot, P., Daburon, V., Nakayama, K.I., Manenti, S., Davy, A., and Besson, A. (2016). p57(Kip2) knock-in mouse reveals CDK-independent contribution in the development of Beckwith-Wiedemann syndrome. *J. Pathol.* *239*, 250–261. <https://doi.org/10.1002/path.4721>.
6. Eggermann, T., Binder, G., Brioude, F., Maher, E.R., Lapunzina, P., Cubellis, M.V., Bergadá, I., Prawitt, D., and Begemann, M. (2014). CDKN1C mutations: two sides of the same coin. *Trends Mol. Med.* *20*, 614–622. <https://doi.org/10.1016/j.molmed.2014.09.001>.
7. Weksberg, R., Shuman, C., and Beckwith, J.B. (2010). Beckwith-Wiedemann syndrome. *Eur. J. Hum. Genet.* *18*, 8–14. <https://doi.org/10.1038/ejhg.2009.106>.
8. Pateras, I.S., Apostolopoulou, K., Niforou, K., Kotsinas, A., and Gorgoulis, V.G. (2009). p57KIP2: "Kip"ing the cell under control. *Mol. Cancer Res.* *7*, 1902–1919. <https://doi.org/10.1158/1541-7786.MCR-09-0317>.
9. Susaki, E., Nakayama, K., Yamasaki, L., and Nakayama, K.I. (2009). Common and specific roles of the related CDK inhibitors p27 and p57 revealed by a knock-in mouse model. *Proc. Natl. Acad. Sci. USA* *106*, 5192–5197. <https://doi.org/10.1073/pnas.0811712106>.
10. Riccio, O., van Gijn, M.E., Bezdek, A.C., Pellegrinet, L., van Es, J.H., Zimmer-Strobl, U., Strobl, L.J., Honjo, T., Clevers, H., and Radtke, F. (2008). Loss of intestinal crypt progenitor cells owing to inactivation of both Notch1 and Notch2 is accompanied by derepression of CDK inhibitors p27Kip1 and p57Kip2. *EMBO Rep.* *9*, 377–383. <https://doi.org/10.1038/embor.2008.7>.
11. Barriga, F.M., Montagni, E., Mana, M., Mendez-Lago, M., Hernando-Mombona, X., Sevillano, M., Guillaumet-Adkins, A., Rodriguez-Esteban, G., Buczacki, S.J.A., Gut, M., et al. (2017). Mex3a marks a slowly dividing

#### Figure 7. p57 participate in the recruitment of a corepressor complex on Ascl2 target promoters

(A–D) ChIP experiments to determine the presence of a corepressor complex on Ascl2 target promoters. ChIP using antibodies against Ascl2 (A), p57 (B), mSin3a (C), and HDAC7 (D), or isotype control, were followed by qPCR with primers specific for the Lgr5, Sox9, or EphB3 promoters or for an unrelated intergenic region as negative control. Results are expressed as a percentage of input. Graphs display the results of one representative assay from three independent experiments and the two other experiments are provided in [Figures S8A–S8D](#).

(E–H) Pull-down assays with streptavidin beads bound to biotinylated oligonucleotides derived from the E-box containing region of the Lgr5 promoter or to oligonucleotides in which point mutations disrupt the E-box as negative control were performed on cell lysate from HEK293 transfected with Ascl2 and p57 (E); p57<sup>CK−</sup> (F); p57, Ascl2, and HDAC7 (G); or mSin3a (H). The presence of the different proteins was assessed by immunoblotting. Corresponding levels of transfected proteins in the extracts are shown. β-Actin was used as loading control.

(I) p57 silencing in SW480 cells. SW480 cells were transfected with control or p57 siRNA for 48 h and subjected to immunoblot for p57. β-Actin was used as loading control. Graph shows mean p57 silencing ±SEM from four independent experiments. Unpaired two-tailed Student's t test, \*\*\*p ≤ 0.001.

(J) ChIP with HDAC7 antibodies or control IgG in SW480 cells transfected for 48 h with control or p57 siRNA followed by qPCR with primers specific for the Lgr5, Sox9, and EphB3 promoters or for an unrelated intergenic region as negative control. Results are expressed as a percentage of input. Graph displays the results of one representative assay from three independent experiments, and the two other experiments are provided in [Figure S8E](#).

(K) ChIP with H3K27-Ac antibodies or control IgG in SW480 cells transfected for 48 h with control or p57 siRNA followed by qPCR with primers specific for the Lgr5, Sox9, and EphB3 promoters or for an unrelated intergenic region as negative control. Results are expressed as a percentage of input. Graph displays the results of one representative assay from four independent experiments, and the two other experiments are provided in [Figure S8F](#). See also [Figure S8](#).

- subpopulation of Lgr5+ intestinal stem cells. *Cell Stem Cell* 20, 801–816.e7. <https://doi.org/10.1016/j.stem.2017.02.007>.
12. Higa, T., Okita, Y., Matsumoto, A., Nakayama, S., Oka, T., Sugahara, O., Koga, D., Takeishi, S., Nakatsumi, H., Hosen, N., et al. (2022). Spatiotemporal reprogramming of differentiated cells underlies regeneration and neoplasia in the intestinal epithelium. *Nat. Commun.* 13, 1500. <https://doi.org/10.1038/s41467-022-29165-z>.
  13. Clevers, H. (2013). The intestinal crypt, a prototype stem cell compartment. *Cell* 154, 274–284. <https://doi.org/10.1016/j.cell.2013.07.004>.
  14. Beumer, J., and Clevers, H. (2021). Cell fate specification and differentiation in the adult mammalian intestine. *Nat. Rev. Mol. Cell Biol.* 22, 39–53. <https://doi.org/10.1038/s41580-020-0278-0>.
  15. Barker, N., van Es, J.H., Kuipers, J., Kujala, P., van den Born, M., Cozijnsen, M., Haegebarth, A., Korving, J., Begthel, H., Peters, P.J., and Clevers, H. (2007). Identification of stem cells in small intestine and colon by marker gene Lgr5. *Nature* 449, 1003–1007. <https://doi.org/10.1038/nature06196>.
  16. Grosse, A.S., Pressprich, M.F., Curley, L.B., Hamilton, K.L., Margolis, B., Hildebrand, J.D., and Gumucio, D.L. (2011). Cell dynamics in fetal intestinal epithelium: implications for intestinal growth and morphogenesis. *Development* 138, 4423–4432. <https://doi.org/10.1242/dev.065789>.
  17. Wells, J.M., and Spence, J.R. (2014). How to make an intestine. *Development* 141, 752–760. <https://doi.org/10.1242/dev.097386>.
  18. Baulies, A., Angelis, N., and Li, V.S.W. (2020). Hallmarks of intestinal stem cells. *Development* 147, dev182675. <https://doi.org/10.1242/dev.182675>.
  19. Nigmatullina, L., Norkin, M., Dzama, M.M., Messner, B., Sayols, S., and Soshnikova, N. (2017). Id2 controls specification of Lgr5(+) intestinal stem cell progenitors during gut development. *EMBO J.* 36, 869–885. <https://doi.org/10.15252/embj.201694959>.
  20. Snippert, H.J., van der Flier, L.G., Sato, T., van Es, J.H., van den Born, M., Kroon-Veenboer, C., Barker, N., Klein, A.M., van Rheenen, J., Simons, B.D., and Clevers, H. (2010). Intestinal crypt homeostasis results from neutral competition between symmetrically dividing Lgr5 stem cells. *Cell* 143, 134–144. <https://doi.org/10.1016/j.cell.2010.09.016>.
  21. Barker, N. (2014). Adult intestinal stem cells: critical drivers of epithelial homeostasis and regeneration. *Nat. Rev. Mol. Cell Biol.* 15, 19–33. <https://doi.org/10.1038/nrm3721>.
  22. Tan, S.H., Phuah, P., Tan, L.T., Yada, S., Goh, J., Tomaz, L.B., Chua, M., Wong, E., Lee, B., and Barker, N. (2021). A constant pool of Lgr5(+) intestinal stem cells is required for intestinal homeostasis. *Cell Rep.* 34, 108633. <https://doi.org/10.1016/j.celrep.2020.108633>.
  23. Shivdasani, R.A., Clevers, H., and de Sauvage, F.J. (2021). Tissue regeneration: reserve or reverse? *Science* 371, 784–786. <https://doi.org/10.1126/science.abb6848>.
  24. Bankaitis, E.D., Ha, A., Kuo, C.J., and Magness, S.T. (2018). Reserve stem cells in intestinal homeostasis and injury. *Gastroenterology* 155, 1348–1361. <https://doi.org/10.1053/j.gastro.2018.08.016>.
  25. Tian, H., Biehs, B., Warming, S., Leong, K.G., Rangell, L., Klein, O.D., and de Sauvage, F.J. (2011). A reserve stem cell population in small intestine renders Lgr5-positive cells dispensable. *Nature* 478, 255–259. <https://doi.org/10.1038/nature10408>.
  26. Sangiorgi, E., and Capecchi, M.R. (2008). Bmi1 is expressed in vivo in intestinal stem cells. *Nat. Genet.* 40, 915–920. <https://doi.org/10.1038/ng.165>.
  27. Yan, K.S., Chia, L.A., Li, X., Ootani, A., Su, J., Lee, J.Y., Su, N., Luo, Y., Heilshorn, S.C., Amieva, M.R., et al. (2012). The intestinal stem cell markers Bmi1 and Lgr5 identify two functionally distinct populations. *Proc. Natl. Acad. Sci. USA* 109, 466–471. <https://doi.org/10.1073/pnas.1118857109>.
  28. Montgomery, R.K., Carlone, D.L., Richmond, C.A., Farilla, L., Kranendonk, M.E.G., Henderson, D.E., Baffour-Awuah, N.Y., Ambruzs, D.M., Fogli, L.K., Algra, S., and Breault, D.T. (2011). Mouse telomerase reverse transcriptase (mTert) expression marks slowly cycling intestinal stem cells. *Proc. Natl. Acad. Sci. USA* 108, 179–184. <https://doi.org/10.1073/pnas.1013004108>.
  29. Takeda, N., Jain, R., LeBoeuf, M.R., Wang, Q., Lu, M.M., and Epstein, J.A. (2011). Interconversion between intestinal stem cell populations in distinct niches. *Science* 334, 1420–1424. <https://doi.org/10.1126/science.1213214>.
  30. Formeister, E.J., Sionas, A.L., Lorange, D.K., Barkley, C.L., Lee, G.H., and Magness, S.T. (2009). Distinct SOX9 levels differentially mark stem/progenitor populations and enteroendocrine cells of the small intestine epithelium. *Am. J. Physiol. Gastrointest. Liver Physiol.* 296, G1108–G1118. <https://doi.org/10.1152/ajpgi.00004.2009>.
  31. Van Landeghem, L., Santoro, M.A., Krebs, A.E., Mah, A.T., Dehmer, J.J., Gracz, A.D., Scull, B.P., McNaughton, K., Magness, S.T., and Lund, P.K. (2012). Activation of two distinct Sox9-EGFP-expressing intestinal stem cell populations during crypt regeneration after irradiation. *Am. J. Physiol. Gastrointest. Liver Physiol.* 302, G1111–G1132. <https://doi.org/10.1152/ajpgi.00519.2011>.
  32. Ayyaz, A., Kumar, S., Sangiorgi, B., Ghoshal, B., Gosio, J., Ouladan, S., Fink, M., Barutcu, S., Trcka, D., Shen, J., et al. (2019). Single-cell transcriptomes of the regenerating intestine reveal a revival stem cell. *Nature* 569, 121–125. <https://doi.org/10.1038/s41586-019-1154-y>.
  33. Muñoz, J., Stange, D.E., Schepers, A.G., van de Wetering, M., Koo, B.K., Itzkovitz, S., Volckmann, R., Kung, K.S., Koster, J., Radulescu, S., et al. (2012). The Lgr5 intestinal stem cell signature: robust expression of proposed quiescent '+4' cell markers. *EMBO J.* 31, 3079–3091. <https://doi.org/10.1038/emboj.2012.166>.
  34. Itzkovitz, S., Lyubimova, A., Blat, I.C., Maynard, M., van Es, J., Lees, J., Jacks, T., Clevers, H., and van Oudenaarden, A. (2011). Single-molecule transcript counting of stem-cell markers in the mouse intestine. *Nat. Cell Biol.* 14, 106–114. <https://doi.org/10.1038/ncb2384>.
  35. Li, N., Yousefi, M., Nakauka-Ddamba, A., Jain, R., Tobias, J., Epstein, J.A., Jensen, S.T., and Lengner, C.J. (2014). Single-cell analysis of proxy reporter allele-marked epithelial cells establishes intestinal stem cell hierarchy. *Stem Cell Rep.* 3, 876–891. <https://doi.org/10.1016/j.stemcr.2014.09.011>.
  36. Buczacck, S.J.A., Zecchini, H.I., Nicholson, A.M., Russell, R., Vermeulen, L., Kemp, R., and Winton, D.J. (2013). Intestinal label-retaining cells are secretory precursors expressing Lgr5. *Nature* 495, 65–69. <https://doi.org/10.1038/nature11965>.
  37. Basak, O., van de Born, M., Korving, J., Beumer, J., van der Elst, S., van Es, J.H., and Clevers, H. (2014). Mapping early fate determination in Lgr5+ crypt stem cells using a novel Ki67-RFP allele. *EMBO J.* 33, 2057–2068. <https://doi.org/10.15252/embj.201488017>.
  38. Tetteh, P.W., Basak, O., Farin, H.F., Wiebrands, K., Kretzschmar, K., Begthel, H., van den Born, M., Korving, J., de Sauvage, F., van Es, J.H., et al. (2016). Replacement of lost Lgr5-positive stem cells through plasticity of their enterocyte-lineage daughters. *Cell Stem Cell* 18, 203–213. <https://doi.org/10.1016/j.stem.2016.01.001>.
  39. van Es, J.H., Sato, T., van de Wetering, M., Lyubimova, A., Yee Nee, A.N., Gregorieff, A., Sasaki, N., Zeinstra, L., van den Born, M., Korving, J., et al. (2012). Dll1+ secretory progenitor cells revert to stem cells upon crypt damage. *Nat. Cell Biol.* 14, 1099–1104. <https://doi.org/10.1038/ncb2581>.
  40. Murata, K., Jadhav, U., Madha, S., van Es, J., Dean, J., Cavazza, A., Wucherpfennig, K., Michor, F., Clevers, H., and Shivdasani, R.A. (2020). Ascl2-Dependent cell dedifferentiation drives regeneration of ablated intestinal stem cells. *Cell Stem Cell* 26, 377–390.e6. <https://doi.org/10.1016/j.stem.2019.12.011>.
  41. Schuijers, J., Junker, J.P., Mokry, M., Hatzis, P., Koo, B.K., Sasselli, V., van der Flier, L.G., Cuppen, E., van Oudenaarden, A., and Clevers, H. (2015). Ascl2 acts as an R-spondin/Wnt-responsive switch to control stemness in intestinal crypts. *Cell Stem Cell* 16, 158–170. <https://doi.org/10.1016/j.stem.2014.12.006>.
  42. van der Flier, L.G., van Gijn, M.E., Hatzis, P., Kujala, P., Haegebarth, A., Stange, D.E., Begthel, H., van den Born, M., Guryev, V., Oving, I., et al.

- (2009). Transcription factor achaete scute-like 2 controls intestinal stem cell fate. *Cell* 136, 903–912. <https://doi.org/10.1016/j.cell.2009.01.031>.
43. Leushacke, M., Tan, S.H., Wong, A., Swathi, Y., Hajamohideen, A., Tan, L.T., Goh, J., Wong, E., Denil, S.L.I.J., Murakami, K., and Barker, N. (2017). Lgr5-expressing chief cells drive epithelial regeneration and cancer in the oxyntic stomach. *Nat. Cell Biol.* 19, 774–786. <https://doi.org/10.1038/ncb3541>.
  44. van der Flier, L.G., Haegerbarth, A., Stange, D.E., van de Wetering, M., and Clevers, H. (2009). OLFM4 is a robust marker for stem cells in human intestine and marks a subset of colorectal cancer cells. *Gastroenterology* 137, 15–17. <https://doi.org/10.1053/j.gastro.2009.05.035>.
  45. Zhang, N., Yantiss, R.K., Nam, H.S., Chin, Y., Zhou, X.K., Scherl, E.J., Bosworth, B.P., Subbaramaiah, K., Dannenberg, A.J., and Benezra, R. (2014). ID1 is a functional marker for intestinal stem and progenitor cells required for normal response to injury. *Stem Cell Rep.* 3, 716–724. <https://doi.org/10.1016/j.stemcr.2014.09.012>.
  46. Takeda, N., Jain, R., Leboeuf, M.R., Padmanabhan, A., Wang, Q., Li, L., Lu, M.M., Millar, S.E., and Epstein, J.A. (2013). Hopx expression defines a subset of multipotent hair follicle stem cells and a progenitor population primed to give rise to K6+ niche cells. *Development* 140, 1655–1664. <https://doi.org/10.1242/dev.093005>.
  47. Stewart, A.S., Schaaf, C.R., Luff, J.A., Freund, J.M., Becker, T.C., Tufts, S.R., Robertson, J.B., and Gonzalez, L.M. (2021). HOPX(+) injury-resistant intestinal stem cells drive epithelial recovery after severe intestinal ischemia. *Am. J. Physiol. Gastrointest. Liver Physiol.* 321, G588–G602. <https://doi.org/10.1152/ajpgi.00165.2021>.
  48. Wang, Y., Chiang, I.L., Ohara, T.E., Fujii, S., Cheng, J., Muegge, B.D., Ver Heul, A., Han, N.D., Lu, Q., Xiong, S., et al. (2019). Long-term culture captures injury-repair cycles of colonic stem cells. *Cell* 179, 1144–1159.e15. <https://doi.org/10.1016/j.cell.2019.10.015>.
  49. Li, N., Nakauka-Ddamba, A., Tobias, J., Jensen, S.T., and Lengner, C.J. (2016). Mouse label-retaining cells are molecularly and functionally distinct from reserve intestinal stem cells. *Gastroenterology* 151, 298–310.e7. <https://doi.org/10.1053/j.gastro.2016.04.049>.
  50. Roche, K.C., Gracz, A.D., Liu, X.F., Newton, V., Akiyama, H., and Magness, S.T. (2015). SOX9 maintains reserve stem cells and preserves radio-resistance in mouse small intestine. *Gastroenterology* 149, 1553–1563.e10. <https://doi.org/10.1053/j.gastro.2015.07.004>.
  51. Haber, A.L., Biton, M., Rogel, N., Herbst, R.H., Shekhar, K., Smillie, C., Burgin, G., Delorey, T.M., Howitt, M.R., Katz, Y., et al. (2017). A single-cell survey of the small intestinal epithelium. *Nature* 551, 333–339. <https://doi.org/10.1038/nature24489>.
  52. Katz, J.P., Perreault, N., Goldstein, B.G., Lee, C.S., Labosky, P.A., Yang, V.W., and Kaestner, K.H. (2002). The zinc-finger transcription factor Klf4 is required for terminal differentiation of goblet cells in the colon. *Development* 129, 2619–2628. <https://doi.org/10.1242/dev.129.11.2619>.
  53. Katano, T., Bialkowska, A.B., and Yang, V.W. (2020). KLF4 regulates goblet cell differentiation in BMI1(+) reserve intestinal stem cell lineage during homeostasis. *Int. J. Stem Cells* 13, 424–431. <https://doi.org/10.15283/ijsc20048>.
  54. Joseph, B., Andersson, E.R., Vlachos, P., Södersten, E., Liu, L., Teixeira, A.I., and Hermanson, O. (2009). p57Kip2 is a repressor of Mash1 activity and neuronal differentiation in neural stem cells. *Cell Death Differ.* 16, 1256–1265. <https://doi.org/10.1038/cdd.2009.72>.
  55. Reynaud, E.G., Leibovitch, M.P., Tintignac, L.A., Pospel, K., Guillier, M., and Leibovitch, S.A. (2000). Stabilization of MyoD by direct binding to p57(Kip2). *J. Biol. Chem.* 275, 18767–18776.
  56. Reynaud, E.G., Pospel, K., Guillier, M., Leibovitch, M.P., and Leibovitch, S.A. (1999). p57(Kip2) stabilizes the MyoD protein by inhibiting cyclin E-Cdk2 kinase activity in growing myoblasts. *Mol. Cell Biol.* 19, 7621–7629. <https://doi.org/10.1128/MCB.19.11.7621>.
  57. Joaquin, M., and Watson, R.J. (2003). The cell cycle-regulated B-Myb transcription factor overcomes cyclin-dependent kinase inhibitory activity of p57(KIP2) by interacting with its cyclin-binding domain. *J. Biol. Chem.* 278, 44255–44264. <https://doi.org/10.1074/jbc.M308953200>.
  58. Kao, H.Y., Downes, M., Ordentlich, P., and Evans, R.M. (2000). Isolation of a novel histone deacetylase reveals that class I and class II deacetylases promote SMRT-mediated repression. *Genes Dev.* 14, 55–66.
  59. Yan, K.S., Gevaert, O., Zheng, G.X.Y., Anchang, B., Probert, C.S., Larkin, K.A., Davies, P.S., Cheng, Z.F., Kaddis, J.S., Han, A., et al. (2017). Intestinal enteroendocrine lineage cells possess homeostatic and injury-inducible stem cell activity. *Cell Stem Cell* 21, 78–90.e6. <https://doi.org/10.1016/j.stem.2017.06.014>.
  60. Ma, Y., Chen, L., Wright, G.M., Pillai, S.R., Chellappan, S.P., and Cress, W.D. (2010). CDKN1C negatively regulates RNA polymerase II C-terminal domain phosphorylation in an E2F1-dependent manner. *J. Biol. Chem.* 285, 9813–9822. <https://doi.org/10.1074/jbc.M109.091496>.
  61. Kullmann, M.K., Pegka, F., Ploner, C., and Hengst, L. (2021). Stimulation of c-jun/AP-1-activity by the cell cycle inhibitor p57(kip2). *Front. Cell Dev. Biol.* 9, 664609. <https://doi.org/10.3389/fcell.2021.664609>.
  62. Kullmann, M.K., Podmirseg, S.R., Roilo, M., and Hengst, L. (2020). The CDK inhibitor p57(Kip2) enhances the activity of the transcriptional coactivator FHL2. *Sci. Rep.* 10, 7140. <https://doi.org/10.1038/s41598-020-62641-4>.
  63. Pippa, R., Espinosa, L., Gundem, G., García-Escudero, R., Dominguez, A., Orlando, S., Gallastegui, E., Saiz, C., Besson, A., Pujol, M.J., et al. (2012). p27Kip1 represses transcription by direct interaction with p130/E2F4 at the promoters of target genes. *Oncogene* 31, 4207–4220. <https://doi.org/10.1038/onc.2011.582>.
  64. Baulies, A., Angelis, N., Foglizzo, V., Danielsen, E.T., Patel, H., Novellasdemunt, L., Kucharska, A., Carvalho, J., Nye, E., De Coppi, P., and Li, V.S.W. (2020). The transcription Co-repressors MTG8 and MTG16 regulate exit of intestinal stem cells from their niche and differentiation into enterocyte vs secretory lineages. *Gastroenterology* 159, 1328–1341.e3. <https://doi.org/10.1053/j.gastro.2020.06.012>.
  65. Davis, J.N., McGhee, L., and Meyers, S. (2003). The ETO (MTG8) gene family. *Gene* 303, 1–10. [https://doi.org/10.1016/s0378-1119\(02\)01172-1](https://doi.org/10.1016/s0378-1119(02)01172-1).
  66. Saxena, M., and Shivdasani, R.A. (2021). Epigenetic signatures and plasticity of intestinal and other stem cells. *Annu. Rev. Physiol.* 83, 405–427. <https://doi.org/10.1146/annurev-physiol-021119-034520>.
  67. Jadhav, U., Saxena, M., O'Neill, N.K., Saadatpour, A., Yuan, G.C., Herbert, Z., Murata, K., and Shivdasani, R.A. (2017). Dynamic reorganization of chromatin accessibility signatures during dedifferentiation of secretory precursors into Lgr5+ intestinal stem cells. *Cell Stem Cell* 21, 65–77.e5. <https://doi.org/10.1016/j.stem.2017.05.001>.
  68. Kim, T.H., Li, F., Ferreira-Neira, I., Ho, L.L., Luyten, A., Nalapareddy, K., Long, H., Verzi, M., and Shivdasani, R.A. (2014). Broadly permissive intestinal chromatin underlies lateral inhibition and cell plasticity. *Nature* 506, 511–515. <https://doi.org/10.1038/nature12903>.
  69. Jubb, A.M., Chalasani, S., Frantz, G.D., Smits, R., Grabsch, H.I., Kavi, V., Maughan, N.J., Hillan, K.J., Quirke, P., and Koeppen, H. (2006). Achaete-scute like 2 (ascl2) is a target of Wnt signalling and is upregulated in intestinal neoplasia. *Oncogene* 25, 3445–3457. <https://doi.org/10.1038/sj.onc.1209382>.
  70. Giakountis, A., Moulos, P., Zarkou, V., Oikonomou, C., Harokopos, V., Hatzigeorgiou, A.G., Reczko, M., and Hatzis, P. (2016). A positive regulatory loop between a Wnt-regulated non-coding RNA and ASCL2 controls intestinal stem cell fate. *Cell Rep.* 15, 2588–2596. <https://doi.org/10.1016/j.celrep.2016.05.038>.
  71. Tanaka, T., Kojima, K., Yokota, K., Tanaka, Y., Ooizumi, Y., Ishii, S., Nishizawa, N., Yokoi, K., Ushiku, H., Kikuchi, M., et al. (2019). Comprehensive genetic search to clarify the molecular mechanism of drug resistance identifies ASCL2-LEF1/TSPAN8 Axis in colorectal cancer. *Ann. Surg. Oncol.* 26, 1401–1411. <https://doi.org/10.1245/s10434-019-07172-7>.

72. Li, J.Q., Wu, F., Usuki, H., Kubo, A., Masaki, T., Fujita, J., Bandoh, S., Saoo, K., Takeuchi, H., Kuriyama, S., et al. (2003). Loss of p57KIP2 is associated with colorectal carcinogenesis. *Int. J. Oncol.* **23**, 1537–1543.
73. Ma, Z., Gu, S., Song, M., Yan, C., Hui, B., Ji, H., Wang, J., Zhang, J., Wang, K., and Zhao, Q. (2017). Long non-coding RNA SNHG17 is an unfavourable prognostic factor and promotes cell proliferation by epigenetically silencing P57 in colorectal cancer. *Mol. Biosyst.* **13**, 2350–2361. <https://doi.org/10.1039/c7mb00280g>.
74. Borriello, A., Caldarelli, I., Bencivenga, D., Crisculo, M., Cucciolla, V., Tramontano, A., Oliva, A., Perrotta, S., and Della Ragione, F. (2011). p57(Kip2) and cancer: time for a critical appraisal. *Mol. Cancer Res.* **9**, 1269–1284. <https://doi.org/10.1158/1541-7786.MCR-11-0220>.
75. Weis, B., Schmidt, J., Maamar, H., Raj, A., Lin, H., Tóth, C., Riedmann, K., Raddatz, G., Seitz, H.K., Ho, A.D., et al. (2015). Inhibition of intestinal tumor formation by deletion of the DNA methyltransferase 3a. *Oncogene* **34**, 1822–1830. <https://doi.org/10.1038/onc.2014.114>.
76. Shiokawa, D., Sakai, H., Ohata, H., Miyazaki, T., Kanda, Y., Sekine, S., Narushima, D., Hosokawa, M., Kato, M., Suzuki, Y., et al. (2020). Slow-cycling cancer stem cells regulate progression and chemoresistance in colon cancer. *Cancer Res.* **80**, 4451–4464. <https://doi.org/10.1158/0008-5472.CAN-20-0378>.
77. Tomic, G., Morrissey, E., Kozar, S., Ben-Moshe, S., Hoyle, A., Azzarelli, R., Kemp, R., Chilamakuri, C.S.R., Itzkovitz, S., Philpott, A., and Winton, D.J. (2018). Phospho-regulation of ATOH1 is required for plasticity of secretory progenitors and tissue regeneration. *Cell Stem Cell* **23**, 436–443.e7. <https://doi.org/10.1016/j.stem.2018.07.002>.
78. Sheng, X., Lin, Z., Lv, C., Shao, C., Bi, X., Deng, M., Xu, J., Guerrero-Juarez, C.F., Li, M., Wu, X., et al. (2020). Cycling stem cells are radioresistant and regenerate the intestine. *Cell Rep.* **32**, 107952. <https://doi.org/10.1016/j.celrep.2020.107952>.
79. Gerbe, F., and Jay, P. (2016). Intestinal tuft cells: epithelial sentinels linking luminal cues to the immune system. *Mucosal Immunol.* **9**, 1353–1359. <https://doi.org/10.1038/mi.2016.68>.
80. Dobin, A., Davis, C.A., Schlesinger, F., Drenkow, J., Zaleski, C., Jha, S., Batut, P., Chaisson, M., and Gingeras, T.R. (2013). STAR: ultrafast universal RNA-seq aligner. *Bioinformatics* **29**, 15–21. <https://doi.org/10.1093/bioinformatics/bts635>.
81. Trapnell, C., Roberts, A., Goff, L., Pertea, G., Kim, D., Kelley, D.R., Pimentel, H., Salzberg, S.L., Rinn, J.L., and Pachter, L. (2012). Differential gene and transcript expression analysis of RNA-seq experiments with TopHat and Cufflinks. *Nat. Protoc.* **7**, 562–578. <https://doi.org/10.1038/nprot.2012.016>.
82. Anders, S., and Huber, W. (2010). Differential expression analysis for sequence count data. *Genome Biol.* **11**, R106. <https://doi.org/10.1186/gb-2010-11-10-r106>.
83. Love, M.I., Huber, W., and Anders, S. (2014). Moderated estimation of fold change and dispersion for RNA-seq data with DESeq2. *Genome Biol.* **15**, 550. <https://doi.org/10.1186/s13059-014-0550-8>.

STAR★METHODS

KEY RESOURCES TABLE

REAGENT or RESOURCE	SOURCE	IDENTIFIER
<b>Antibodies</b>		
Mouse anti-PCNA (PC10, Cat# sc-56)	Santa Cruz Biotechnology	RRID:AB_628110
Mouse anti-mSin3a (G-11, Cat# sc-5299)	Santa Cruz Biotechnology	RRID:AB_2187766
Mouse anti-HDAC7 (A-7, Cat# sc-74563)	Santa Cruz Biotechnology	RRID:AB_2248191
Mouse anti-Myc (9E10, Cat# sc-40)	Santa Cruz Biotechnology	RRID:AB_627268
Mouse anti-OctA-probe (Flag, H5, Cat# sc-166355)	Santa Cruz Biotechnology	RRID:AB_2017593
Mouse anti-Actin (C4, Cat# sc-47778)	Santa Cruz Biotechnology	RRID:AB_626632
Rabbit anti-p57 (H-91, Cat# sc-8298)	Santa Cruz Biotechnology	RRID:AB_2078155
Rabbit anti-Myc (A-14, Cat# sc-789)	Santa Cruz Biotechnology	RRID:AB_631274
Mouse anti-Ascl2 (8F1, Cat# MAB4417)	Merck Millipore	RRID:AB_10562654
Rabbit anti-Sox9 (Cat# AB5535)	Merck Millipore	RRID:AB_2239761
Rabbit anti-p57Kip2 (Cat# 06556)	Merck Millipore	RRID:AB_310168
Mouse anti-β Actin (Cat# A2228)	Merck Millipore	RRID:AB_476697
rabbit anti-Ascl2 (Cat# SAB1305026)	Merck Millipore	RRID:AB_2934057
Rabbit anti-mSin3a (PA1-870)	Thermo Scientific	RRID:AB_2187625
Rabbit anti-HDAC7 (PA5-29937)	Thermo Scientific	RRID:AB_2547411
Rabbit anti-Ki-67 (SP6, RM-9106-S1)	Thermo Scientific	RRID:AB_2341197
Rabbit anti-cleaved caspase 3 (Cat# 9664)	Cell Signaling Technology	RRID:AB_2070042
Rabbit anti-Olfm4 (Cat# 39141)	Cell Signaling Technology	RRID:AB_2650511
Rabbit anti-p57 (Cat# 2557S)	Cell Signaling Technology	RRID:AB_2291591
Rabbit anti-DYKDDDK (Flag) (Cat# 2368)	Cell Signaling Technology	RRID:AB_2217020
Rabbit anti-HDAC7 (Cat# 10831)	Cell Signaling Technology	RRID:AB_2797731
Rabbit anti-turboGFP (Cat# AB513)	Evrogen	RRID:AB_2934059
Goat anti-GFP (Cat# GTX26673)	Genetex	RRID:AB_371426
Rabbit anti-Id1 (Cat# BCH-1/#37-2)	BioCheck	RRID:AB_2713996
Mouse anti-Grb2 (Cat# 610112)	BD Biosciences	RRID:AB_397518
Mouse anti-E-cadherin (Cat# 610182)	BD Biosciences	RRID:AB_397581
Rabbit anti-histone H3 acetyl K27 (Cat# ab4729)	Abcam	RRID:AB_2118291
Myc-Trap agarose (Cat# yta-20)	Chromotek	RRID:AB_2631369
Peroxidase-AffiniPure Donkey Anti-Mouse IgG (Cat# 715-035-150)	Jackson ImmunoResearch Labs	RRID:AB_2340770
Peroxidase-AffiniPure Donkey Anti-Rabbit IgG (H + L) (Cat# 711-035-152)	Jackson ImmunoResearch Labs	RRID:AB_10015282
Cy2-AffiniPure Donkey Anti-Mouse IgG (H + L) (min X Bov,Ck,Gt,GP,Sy Hms,Hrs, Hu,Rb,Shp Sr Prot) (Cat# 715-225-150)	Jackson ImmunoResearch Labs	RRID:AB_2340826
Cy5-AffiniPure Donkey Anti-Mouse IgG (H + L) (min X Bov,Ck,Gt,GP,Sy Hms,Hrs, Hu,Rb,Shp Sr Prot) (Cat# 715-175-150)	Jackson ImmunoResearch Labs	RRID:AB_2340819
Cy3-AffiniPure Donkey Anti-Mouse IgG (H + L) (min X Bov,Ck,Gt,GP,Sy Hms,Hrs, Hu,Rb,Shp Sr Prot) (Cat# 715-165-150)	Jackson ImmunoResearch Labs	RRID:AB_2340813
Cy <sup>TM</sup> 2 AffiniPure Donkey Anti-Rabbit IgG (H + L) (min X Bov, Ck, Gt, GP, Sy Hms, Hrs, Hu, Ms, Rat, Shp Sr Prot) (Cat# 711-225-152)	Jackson ImmunoResearch Labs	RRID:AB_2340612

(Continued on next page)

**Continued**

REAGENT or RESOURCE	SOURCE	IDENTIFIER
Cy3-AffiniPure Donkey Anti-Rabbit IgG (H + L) (min X Bov,Ck,Gt,GP,Sy Hms,Hrs,Hu,Ms,Rat, Shp Sr Prot) (Cat# 711-165-152)	Jackson ImmunoResearch Labs	RRID:AB_2307443
Cy2-AffiniPure Donkey Anti-Goat IgG (H + L) (min X Ck,GP,Sy Hms,Hrs,Hu,Ms,Rb,Rat Sr Prot) (Cat# 705-225-147)	Jackson ImmunoResearch Labs	RRID:AB_2307341
Cy <sup>TM</sup> 3 AffiniPure Donkey Anti-Goat IgG (H + L) (Cat# 705-165-147)	Jackson ImmunoResearch Labs	RRID:AB_2307351
<b>Chemicals, peptides, and recombinant proteins</b>		
Phalloidin-Fluorophores-495 (Cat# FP-47548A)	Interchim	Cat# FP-47548A
7AAD (Cat# A9400)	Sigma	CAS Number: 7240-37-1
Anti-Rabbit ImmPress Reagent (Cat# MP-7401)	Vector Laboratories	RRID:AB_2336529
ImmPACT DAB (Cat# SK-4105)	Vector Laboratories	RRID:AB_2336520
Dispase (Cat# D4693)	Sigma	CAS Number: 42613-33-2
DNase I (Cat# 1307)	Euromedex	CAS Number: 9003-98-9
TriReagent (Cat# T9424)	Sigma	Cat# T9424
Streptavidin agarose beads (Cat# S1638)	Millipore	Cat# S1638
Magna Chip Protein A/G magnetic beads (Cat# 16-663)	Millipore	Cat# 16-663
IPure v2 kit (Cat# C03010015)	Diagenode	Cat# C03010015
<b>Deposited data</b>		
RNA-Seq data	This paper	GEO: GSE179664
<b>Experimental models: Cell lines</b>		
SW480 colorectal cancer cells	Cell Lines Service	RRID:CVCL_0546
HEK293 cells	Cell Lines Service	RRID:CVCL_0045
<b>Experimental models: Organisms/strains</b>		
Mouse: p57 knockout	Susaki et al. <sup>9</sup>	N/A
Mouse: p57CK-	Duquesnes et al. <sup>5</sup>	N/A
Mouse: Lgr5-eGFP-CreERT2	The Jackson Laboratory	JAX: 008875
Mouse: Hox-3xFlag-GFP	The Jackson Laboratory	JAX: 029271
<b>Oligonucleotides</b>		
Sequences and information about oligonucleotides used in this study are provided in <a href="#">Table S3</a>	N/A	N/A
<b>Recombinant DNA</b>		
pcDNA3.1+Hygro Myc-p57 (mouse)	Duquesnes et al. <sup>5</sup>	N/A
pcDNA3.1+Hygro Myc-p57CK- (mouse)	Duquesnes et al. <sup>5</sup>	N/A
pcDNA3.1+Hygro turboGFP-Ascl2 (mouse)	This paper	N/A
pZs-Green1-DR vector	Clontech	N/A
pZsGreen DA (no promoter)	This paper	N/A
pZs-Green-pGAPDH	This paper	N/A
pZs-Green-pLgr5	This paper	N/A
pZs-Green-pSox9	This paper	N/A
pZs-Green-pPhox2a	This paper	N/A
pcDNA3.1+ HDAC7	Fischle et al. <sup>77</sup>	RRID:Addgene_13824
pCS2+MT-mSin3a	Gift from Bob Eisenman (Addgene plasmid # 30452)	RRID:Addgene_30452

**RESOURCE AVAILABILITY**

**Lead contact**

Further information and requests for resources and reagents should be directed to and will be fulfilled by the lead contact, Arnaud Besson ([arnaud.besson@cnrs.fr](mailto:arnaud.besson@cnrs.fr)).

### Materials availability

Reagents used in this study are publicly available or available from the [lead contact](#) upon reasonable request.

### Data and code availability

- RNA-seq data have been deposited at GEO and are publicly available as of the date of publication. Accession number is listed in the [key resources table](#). Original western blot images and microscopy data reported in this paper will be shared by the [lead contact](#) upon request.
- This paper does not report original code.
- Any additional information required to reanalyze the data reported in this paper is available from the [lead contact](#) upon request.

## EXPERIMENTAL MODEL AND SUBJECT DETAILS

### Mouse models

p57<sup>KO</sup> and p57<sup>CK-</sup> mice have been described previously.<sup>5,9</sup> Mice were maintained in a 129S4/C57BL6J genetic background. They were crossed with Lgr5<sup>+eGFP-CreERT</sup> (JAX #008875) or homozygous Hopx<sup>3xFlag-GFP</sup> (JAX #029271) mice maintained in a C57BL6J genetic background. Both sexes were used and analyzed in this study. Tissues were collected from E18.5 embryos, unless mentioned otherwise, as indicated in figure legends. Mouse husbandry and procedures were performed in accordance with EU and national regulation (Protocol Authorization APAFIS #31318-202104121433391).

The *Cdkn1c* gene is paternally imprinted and p57 is expressed only from the maternal allele. Therefore, maternal inheritance of the mutant allele (p57<sup>+/-m</sup> or p57<sup>+/CK-m</sup>) causes phenotypes similar to homozygous mutations.<sup>4,5</sup> To simplify notations, p57<sup>+/-m</sup> and p57<sup>-/-</sup> mice are referred to as p57<sup>KO</sup>, and p57<sup>+/CK-m</sup> and p57<sup>CK-/CK-</sup> animals are referred to as p57<sup>CK-</sup>.

### Cell culture and transfection

HEK293 cells were grown in DMEM 4.5 g/L glucose (D6429, Sigma) supplemented with 10% Fetal Bovine Serum (FBS) (10270106, Life Technologies), 0.1 mM non-essential amino acid (M7145, Sigma) and 2 μg/mL penicillin/streptomycin (P4333, Sigma). SW480 cells were cultivated in RPMI 2 g/L glucose (R8758, Sigma) supplemented with 10% FBS, 0.1 mM non-essential amino acid, 2 μg/mL penicillin/streptomycin and 2.5 g/L D-Glucose (G7021, Sigma). All cells were grown at 37°C and 5% CO<sub>2</sub>. HEK293 cells were transfected by the calcium phosphate method 24 h prior to lysis. siRNA transfection was performed 48 h before experiments using Interferin (Polyplus transfection) and 50 nM of the indicated siRNA according to the manufacturer's instructions.

## METHOD DETAILS

### Histology

Intestines were collected at E18.5 and fixed in 10% neutral buffered formalin for 2 h at 4°C. For cryosectioning, tissues were incubated in 30% sucrose overnight at 4°C and embedded in OCT (LAMB/OCT, Thermo Scientific). Sections of 12-μm thickness were cut on a cryotome (Cryostat Leica CM1950), placed on Superfrost Plus glass slide (Thermo Scientific) and kept at -20°C. Sections were thawed, rehydrated and blocked in PBS-10% Donkey Serum. Tissues were incubated with primary antibodies overnight at 4°C, washed three times 5 min in PBS 0.1% Triton X-100, then incubated with corresponding secondary antibodies conjugated to Cy2 or -3 for 30 min at room temperature. DNA was stained with Hoechst 33342 (0.1 μg/mL) and slides were mounted with Gelvatol (20% v/v glycerol, 10% w/v polyvinyl alcohol, 70 mM Tris, pH 8). Images of cryosections were acquired on an inverted Leica Sp8 confocal microscope or an inverted spinning disk DM18 Leica microscope equipped with a confocal Yokogawa head CSI-X1-M1N, and processed with the Fiji Software.

Tissues embedded in paraffin were sectioned on a Microm Microtech microtome and serial 5 μm sections were cut and placed on Superfrost Plus slides. Tissues were deparaffinized and stained with hematoxylin and eosin or used for immunostaining. Intestine sections were rehydrated and antigens were unmasked for 30 min in a steamer with sodium citrate (10 mM, pH 6) (Ki67, GFP, p57, PCNA, cleaved caspase 3) or High pH (H-3301, Vector Laboratories) (Olfm4, Sox9, Id1, PCNA) solutions. Slides were washed twice in PBS 0.2% Triton X-100 and once in PBS and then blocked for 0.5 to 2 h in PBS 0.2% Triton X-100, 10% Donkey Serum, 3% BSA solution at room temperature in a humid chamber. Sections were incubated with primary antibodies overnight at 4°C or 1 h at 37°C and washed three times 5 min in PBS 0.2% Triton X-100. For immunofluorescence, sections were incubated with secondary antibodies conjugated to Cy2 and/or Cy3 diluted at 1/400 for 30 min at 37°C, and washed three times 5 min in PBS. DNA was stained with Hoechst 33342 (0.1 μg/mL) in the first wash and slides were mounted with Gelvatol. For immunohistochemistry, sections were incubated with anti-Rabbit ImmPress Reagent (MP-7401, Vector Laboratories) for 30 min at 37°C, washed three times 5 min in PBS 0.2% Triton X-100 and staining was visualized with the chromogen 3'-diaminobenzidine (ImmPACT DAB, SK-4105, Vector Laboratories). Slides were then dehydrated and mounted with PermOUNT mounting medium (SP15-500, Fisher Scientific). Images of paraffin sections were acquired on a Nikon 90i Eclipse microscope using a Digital DS-Fi1 camera (Nikon) or DS-Qi2 HQ Camera (Nikon) and the NIS Element BR Software.

### Flow cytometry

Intestines were dissected at E18.5, minced with a razor blade and incubated with Dispase (1 U/mL) (D4693, Sigma) and DNase I (0.1 mg/mL) (1307, Euromedex) in PBS for 10 min at 37°C under agitation. Single cell suspensions were collected, filtered through a 40- $\mu$ m mesh and washed once in PBS after centrifugation for 10 min at 2000 rpm. Pelleted cells were resuspended in PBS 2% FBS and dead cells were stained with 7AAD (0.5  $\mu$ g/mL) (A9400, Sigma) for 30 min at 4°C. Flow cytometry analyses were performed on a Cytoflex S cytometer (Beckman Coulter) and data were analyzed with the FlowJo software. To monitor GFP populations in reporter mice, a gate was drawn on single live cells. Single cells were identified using Forward Side Scatter and live cells using 7AAD staining (7AAD<sup>-</sup>). All analyses were carried out genotype blind.

### Cell sorting

Intestinal crypts were purified as previously described.<sup>79</sup> Briefly, small intestines were dissected and opened longitudinally. The tissue was incubated with HBSS 30 mM EDTA pH 7.4 for 15 min at 37°C. The epithelium was detached from the mucosa by vigorous shaking and the epithelial fraction was incubated in 10 mL HBSS supplemented with DNase I (0.1 mg/mL) and Dispase (1 U/mL) for 20 min at 37°C. Before sorting, a single cell preparation was obtained by centrifugation and resuspension in HBSS 5% FBS and filtering through a 40- $\mu$ m sieve. Cells were stained with 7AAD (0.5  $\mu$ g/mL) to exclude dead cells. Single GFP<sup>+</sup> 7AAD<sup>-</sup> cells were sorted directly in trizol using a FACSAria Fusion cytometer (Becton Dickinson) for subsequent RNA extraction.

### Reverse transcriptase and qPCR

Cells were lysed in TriReagent (Sigma, T9424) and RNA was extracted according to the manufacturer's protocol. RNA integrity was verified on 0.8% agarose gel and quantified using a Nanodrop spectrophotometer. cDNA was synthesized using SuperScript IV (Thermo Fisher) reverse transcriptase according to the supplier's instructions with 1  $\mu$ g RNA. A negative control without reverse transcriptase was performed for each experiment. qPCR reactions were carried out on a Biorad CFX94 apparatus using Supermix SsoFast EvaGreen (Biorad) with primers at a final concentration of 500 nM and a quantity of cDNA corresponding to 5 ng of RNA per reaction. Ct values were generated with BioRad CFX96 Real-Time PCR software and data were analyzed and normalized using the  $2^{-\Delta\Delta Ct}$  method with GAPDH as housekeeping gene. All Ct were expressed relative to expression in the GFP<sup>Neg</sup> population in the same experiment. The primers used are presented in the Key Resource Table.

### Co-immunoprecipitation

Cells were scrapped and lysed in IP buffer (HEPES 50 mM pH 7.5, NaCl 150 mM, EDTA 1 mM, EGTA 2.5 mM, NP-40 1%, Tween 20 0.1%, glycerol 10%, supplemented with, dithiothreitol 1 mM, phosphatase inhibitors ( $\beta$ -glycerophosphate, NaF and sodium orthovanadate at 10 mM each) and protease inhibitors (Aprotinin, Bestatin, Leupeptin and Pepstatin A, each at 10  $\mu$ g/mL). Lysates were sonicated for 10 s and centrifuged at 12500 g for 5 min at 4°C. Supernatants were collected and the protein concentration was determined by Bradford assay. The lysates (1 mg for SW480, 200  $\mu$ g for HEK293) were incubated with 3  $\mu$ g of the indicated antibodies and 12  $\mu$ L protein Sepharose beads (IPA300, Repligen) at 4°C for 4 h. Beads were washed 4 times with 750  $\mu$ L of IP buffer and resuspended in 12  $\mu$ L of Laemmli buffer, boiled for 3 min at 96°C and analyzed by immunoblotting as described below.

### DNA pull-down assays

For DNA pull-down, 80-mer oligonucleotides biotinylated either on the 5' or 3' end containing the E-box of the Lgr5 promoter or a mutated E-box (see [key resources table](#)) were annealed with the corresponding antisense sequence and bound to streptavidin agarose beads (S1638, Millipore). Beads were washed 3 times, blocked for 3 h with salmon sperm DNA at a final concentration of 4  $\mu$ g/ $\mu$ L and washed again 3 times with IP buffer.

HEK 293 cells transfected with the indicated plasmids by the calcium phosphate method for 24 h in P100 plates and lysed in 800  $\mu$ L of IP buffer as described above. Each pull-down consisted of 500  $\mu$ L of IP buffer, 12  $\mu$ L of beads slurry and 80  $\mu$ L of protein lysate. These mixes were incubated under gentle agitation for 4 h at 4°C, rinsed 3 times with IP buffer and resolved on SDS-PAGE. After transfer on polyvinylidene difluoride membrane (PVDF) membranes, pull-downs were analyzed by probing with the indicated antibodies as described below.

### Immunoblotting

Lysates and immunoprecipitates were prepared as described above. Proteins were resolved on 8 to 12% SDS-PAGE gels, depending on protein size, and transferred to PVDF (Immobilon-P, Millipore). Membranes were blocked for 1 h in PBS-T (PBS 0.1% Tween 20), 5% non-fat dry milk and probed with primary antibodies overnight at 4°C under agitation. After three washes in PBS-T, membranes were probed with HRP-conjugated secondary antibodies at 1/10000 dilution. Signals were visualized with chemiluminescence detection reagent (Sigma, Bio-Rad) and autoradiography films (Blue Devil) or on a Fusion Solo S (Vilber) digital acquisition system.

### GFP transcription reporter assays

The transcription reporter vectors pZs-Green-pGAPDH, pZs-Green-pLgr5, pZs-Green-pSox9 and pZs-Green-pPhox2a were generated by cloning the promoter sequences of GAPDH, Sox9, Lgr5 and Phox2a, purchased from GeneCopoeia (Ref. GAPDH-PF02,

HPRM25638-PF02, HPRM13362-PF02 and HPRM13365-PF02, respectively) in the pZs-Green1-DR vector (Clontech). HEK293 cells were seeded in 24-well plates (45000 cells/well) and co-transfected with 100 ng of reporter plasmid (pZsGreen DA [without promoter, negative control], pZsGreen pGAPDH [positive control], pZsGreen pPhox2a [Ascl1 target, negative control], pZsGreen pSox9 or pZsGreen pLgr5 [Ascl2 targets]), 100 ng of pcDNA3.1+ Hygro Ascl2 plasmid and increasing amounts (0, 100 or 200 ng) of pcDNA3.1+ Hygro p57<sup>WT</sup> or pcDNA3.1+ Hygro p57<sup>CK-</sup> plasmid. Medium was changed 24 h after transfection and 24 h later, 9 images per well were captured in phase contrast and fluorescence with an Incucyte FLR automated microscope (Essen Bioscience) equipped with a 20X objective. The number of fluorescent cells (Object confluence) was quantified on each image using the Incucyte Software (v2011A) and values were normalized by the number fluorescent cells obtained with the pGAPDH reporter plasmid in the same condition.

### Chromatin immunoprecipitation

SW480 cells were grown to confluence. Medium was replaced with PBS and cells were fixed with 1% formaldehyde for 10 min under agitation. Crosslink was stopped by adding glycine at a final concentration of 125 mM for 5 min. Cells were rinsed with cold PBS and scraped with PBS containing protease inhibitors (Aprotinin, Bestatin, Leupeptin and Pepstatin A at 10 μg/mL each). After centrifugation for 10 min at 3000 rpm, cell pellets were resuspended and lysed on ice for 30 min using 200 μL of lysis buffer per 1.10<sup>6</sup> cells (10 mM Tris-HCl pH 8, 0.25% Triton X-100, 10 mM EDTA, 0.5 mM EGTA, 10 mM sodium butyrate, supplemented with 20 mM β-glycerophosphate, 10 μM sodium orthovanadate and protease inhibitors at 10 μg/mL). Cells were pipetted 20 times in a Dounce homogenizer on ice. The lysate was centrifuged for 5 min at 3000 rpm and the pellet containing DNA and cross-linked proteins was resuspended in 300 μL sonication buffer per 3.10<sup>6</sup> cells (10 mM Tris-HCl pH 8, 100 mM NaCl, 1 mM EDTA, 0.5 mM EGTA, 10 mM Sodium butyrate, supplemented with 20 mM β-glycerophosphate, 10 μM sodium orthovanadate, 1% SDS and protease inhibitors at 10 μg/mL) and incubated for 10 min on ice. Chromatin was sheared by sonication (16 cycles of 30 s On/20 s Off, 40% amplitude using a Vibra-cell VCX130 Sonicator [Sonics]) on ice. Samples were centrifuged for 10 min at 1400 rpm to eliminate SDS, and the supernatants containing DNA were transferred to new tubes. Chromatin shearing was verified on agarose gel and DNA concentration was determined with a Nanodrop spectrophotometer. For each ChIP, 200 μg of chromatin were used, and 10% of the volume was kept as control input. The volume of IP was completed to 800 μL with sonication buffer and converted to RIPA buffer by adding 80 μL of 10% Triton X-100, 23 μL of 5 M NaCl and 8 μL of sodium deoxycholate (DOC). For each IP, 4 μg of antibodies and 20 μL of Magna Chip Protein A/G magnetic beads (Millipore) were added and samples were incubated overnight on a rotating wheel at 4°C. Samples were washed 3 times with low salt buffer (10 mM Tris-HCl pH 8, 0.1% Triton X-100, 0.1% SDS, 0.1% DOC, 140 mM NaCl, 1 mM EDTA, 0.5 mM EGTA, 10 mM Sodium butyrate, supplemented with 20 mM β-glycerophosphate and 100 μM sodium orthovanadate), three times with high-salt buffer (same as low salt but with 500 mM NaCl), twice with LiCl buffer (0.25 M LiCl, 1% NP-40, 1% DOC, 10 mM Tris-HCl pH 8, 1 mM EDTA, 10 mM Sodium butyrate and 100 μM sodium orthovanadate) and twice with TE buffer (10 mM Tris-HCl, 1 mM EDTA, pH 8). DNA purification and elution was realized with the IPure v2 kit (Diagenode) according to the manufacturer's protocol. qPCRs were performed with 10 ng of DNA per reaction as described above using the following primers.

### Proximity Ligation Assay

PLAs were performed using the Duolink *in situ* fluorescence technology kit (Sigma) according to the manufacturer's instructions. Briefly, SW480 were seeded on glass coverslips at 25000 cells/cm<sup>2</sup> and grown for 2 days. Cells were fixed with 4% PFA for 20 min at 37°C and permeabilized with PBS 0.2% Triton X-100 for 3 min. Coverslips were blocked at 37°C with Duolink blocking solution and incubated with the indicated combinations of primary antibodies for 1 h at 37°C. Coverslips were washed twice in Duolink wash buffer A and incubated with PLA probes, anti-Rabbit PLUS (DUO92002) and anti-Mouse MINUS (DUO92004) for 1 h at 37°C. Duolink detection reagents were used for signal detection. Following the PLA procedure, cells were stained with Phalloidin A488 at 1/500 for 30 min at 37°C and DNA was stained with Hoechst 33342 (0.1 μg/mL). Images were acquired on a Nikon 90i Eclipse microscope using a DS-Qi2 HQ camera. The following antibodies were used in PLA experiments: rabbit anti-p57 (Sigma, P0357, 1/500), Ascl2 (Sigma, SAB1305026, 1/100), HDAC7 (Sigma, SAB4502143, 1/100) and mouse anti-mSin3a (G-11, sc-5299, 1/100), HDAC7 (A-7, sc-74563, 1/100), Ascl2 (Millipore, 8F1, MAB4417, 1/100).

### QUANTIFICATION AND STATISTICAL ANALYSIS

In all figures, n represents the number of independent experiments. Flow cytometry and cell sorting experiments were performed with blind p57 genotype. Statistical analyzes were performed using GraphPad Prism 6.0. Differences between three groups or more were evaluated by ANOVA test followed by Bonferroni multiple comparison test. Differences between two groups were evaluated by unpaired t test with the post-hoc test of Mann-Whitney. Data are presented as ± s.e.m. Symbols used are: ns: p > 0.05; \*: p ≤ 0.05; \*\*: p ≤ 0.01; \*\*\*: p ≤ 0.001; \*\*\*\*: p ≤ 0.0001.

**Data and code availability*****Transcriptomic analyses***

Ten RNA-seq samples were sequenced using Illumina HiSeq (paired-end, 2x150 bp reads) at Genewiz. The quality of each raw sequencing file (fastq) was verified with FastQC (<https://www.bioinformatics.babraham.ac.uk/projects/fastqc/>). For all files adapters were trimmed with Trim Galore (v-0.6.5, [https://www.bioinformatics.babraham.ac.uk/projects/trim\\_galore](https://www.bioinformatics.babraham.ac.uk/projects/trim_galore)) and clean fastq were aligned to the reference mouse genome (mm10) using STAR aligner (STAR\_2.6.1d).<sup>80</sup> FPKM were computed using cufflinks (v2.2.1)<sup>81</sup> with the annotation from Ensembl database (gtf GRCm38.91). Raw read count per sample was computed using HT-seq count (V1.0)<sup>82</sup> on that same annotation database. Then the raw count table was cleaned, and only genes with a total higher than 50 reads aligned over all samples were kept. The remaining raw read count were normalized using the RLE methods and differential analysis was applied per pairs of conditions using DESeq2 (DESeq2 package version: 1.22.2),<sup>83</sup> available as an R package in bioconductor ([www.bioconductor.org](http://www.bioconductor.org)), to generate the log fold change (log<sub>2</sub>FC) values and adjusted p values (Benjamini and Hochberg method) (Table S2). Heatmaps were drawn using R, on FPKM values.

Any additional information required to reanalyze the data reported in this paper is available from the [lead contact](#) upon request. RNA-Seq data have been deposited on the GEO database under accession number GSE179664.

**Cell Reports, Volume 42**

**Supplemental information**

**p57<sup>Kip2</sup> acts as a transcriptional  
corepressor to regulate intestinal  
stem cell fate and proliferation**

**Justine Creff, Ada Nowosad, Anne Prel, Anne Pizzoccaro, Marion Aguirrebengoa, Nicolas Duquesnes, Caroline Callot, Thomas Jungas, Christine Dozier, and Arnaud Besson**

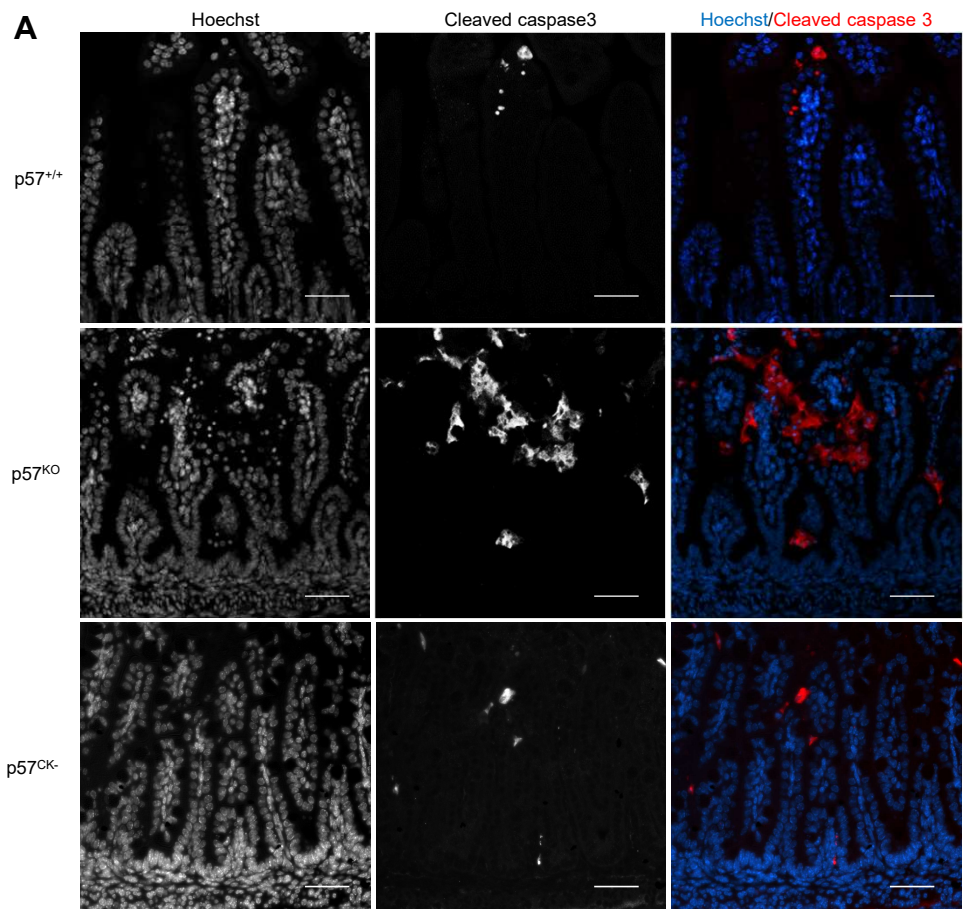
**Table S1:** Intestine length in mm from p57<sup>+/+</sup>, p57<sup>ko</sup> and p57<sup>CK-</sup> E18.5 embryos.

p57 <sup>+/+</sup>	p57 <sup>ko</sup>	p57 <sup>CK-</sup>
121	34	72
123	6	84
112	22	103
114	105	77
119	92	108
122	107	87
103	110	79
111	100	114
94	110	94
95	100	50
99	90	132
93	61	153
98	77	124
102	58	110
108	68	130
99	88	112
75	87	122
72	90	104
86	91	91
80	20	113
92	61	99
83	64	103
95	75	91
91	90	106
103	98	117
105	60	
96	81	
99	89	
110	70	
94		
95		
107		
83		
100		
107		

p57 <sup>+/+</sup>	p57 <sup>ko</sup>	p57 <sup>CK-</sup>
83		
100		
92		
86		
89		
86		
87		
67		
65		
92		
104		
97		
79		
76		
81		
99		
83		
93		
104		
108		
100		
77		
96		
94		
93		

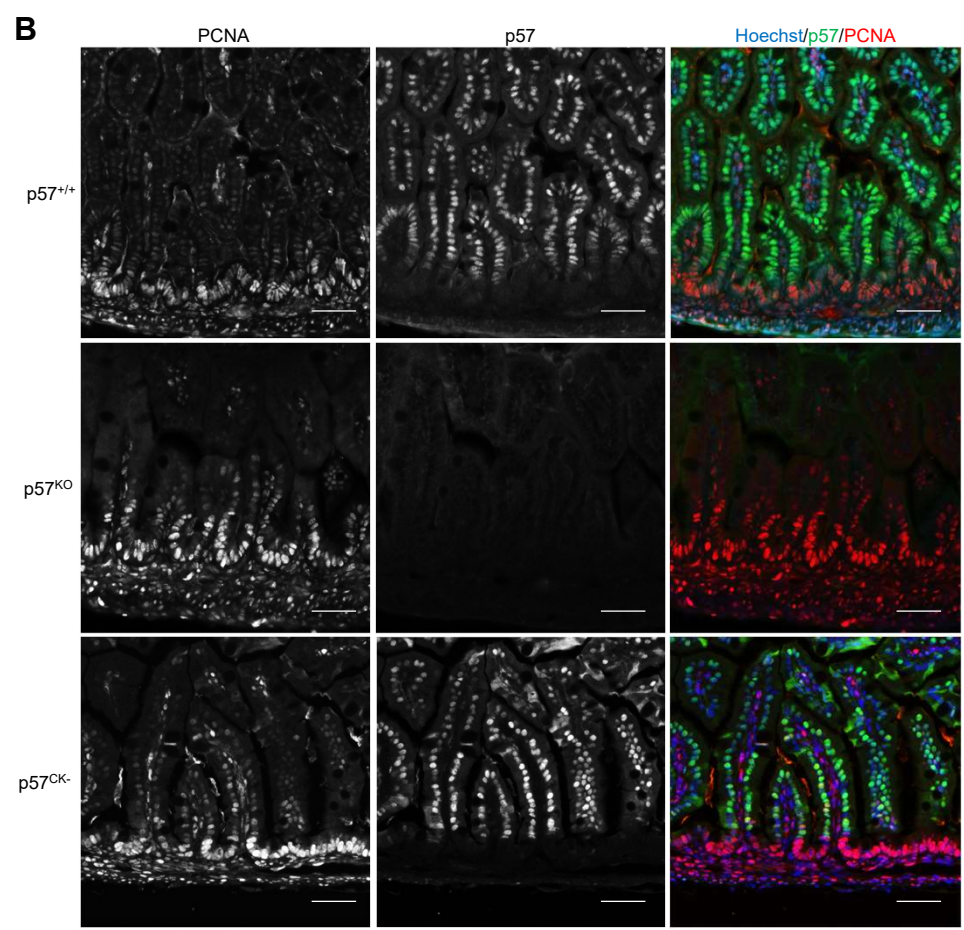
<b>Table S3: Oligonucleotides used in the study</b>		
<b>Oligonucleotide name and sequence (figure number)</b>	<b>Source</b>	<b>Identifier</b>
mp57 Forward CGAGGAGCAGGACGAGAATC (Figure 4)	Eurofins MWG	N/A
mp57 Reverse GAAGAAGTCGTTTCGCATTGGC (Figure 4)	Eurofins MWG	N/A
mMex3a Forward ACACCACGGAGTGCGTTC (Figure S2 and S3)	Eurofins MWG	N/A
mMex3a Reverse GTTGGTTTTGGCCCTCAGA (Figure S2 and S3)	Eurofins MWG	N/A
mLgr5 Forward AGGCTGCCAAAACTTCAGA (Figure S2 and S3)	Eurofins MWG	N/A
mLgr5 Reverse TAACCCAGTCACAGGGAAGG (Figure S2 and S3)	Eurofins MWG	N/A
mAscl2 Forward CCGCGGTAGAGTACATTCGT (Figure S2 and S3)	Eurofins MWG	N/A
mAscl2 Reverse TGCTTTCCTCCGACGAGTAG (Figure S2 and S3)	Eurofins MWG	N/A
mOlfm4 Forward GGACCTGCCAGTGTCTGTT (Figure S2 and S3)	Eurofins MWG	N/A
mOlfm4 Reverse GACCTCTACTCGGACCGTCA (Figure S2 and S3)	Eurofins MWG	N/A
mMuc2 Forward TGATGCCATTGAGGTGGAG (Figure S2 and S3)	Eurofins MWG	N/A
mMuc2 Reverse CTGGCCCTTTGTGTTGTTGC (Figure S2 and S3)	Eurofins MWG	N/A
mMuc4 Forward GCTACAGAGCCAAGTGGACAC (Figure S2 and S3)	Eurofins MWG	N/A
mMuc4 Reverse AAGCCCATGAGCACCCGGTT (Figure S2 and S3)	Eurofins MWG	N/A
mSucrase Forward GCTGGTCGATGGGGAGGA (Figure S2 and S3)	Eurofins MWG	N/A
mSucrase Reverse CCAACGAGCACAGAGGTGGTAT (Figure S2 and S3)	Eurofins MWG	N/A
mAtoh1 Forward GCTTCCTCTGGGGTTACTC (Figure S2 and S3)	Eurofins MWG	N/A
mAtoh1 Reverse CTGTGGGATCTGGGAGATGT (Figure S2 and S3)	Eurofins MWG	N/A
mHes1 Forward CCAGCCAGTGCAACACGA (Figure S2 and S3)	Eurofins MWG	N/A
mHes1 Reverse AATGCCGGGAGCTATCTTTCT (Figure S2 and S3)	Eurofins MWG	N/A
mHopx Forward CTTCAACAAGGTCAACAAGCAC (Figure S2 and S3)	Eurofins MWG	N/A
mHopx Reverse AGGCGCTGCTTAAACCATT (Figure S2 and S3)	Eurofins MWG	N/A

mTert Forward GCAGGTGAACAGCCTCCAGACAG (Figure S2 and S3)	Eurofins MWG	N/A
mTert Reverse TCCTAACACGCTGGTCAAAGGGAAGC (Figure S2 and S3)	Eurofins MWG	N/A
mSox9 Forward AGTACCCGCATCTGCACAAC (Figure S2 and S3)	Eurofins MWG	N/A
mSox9 Reverse CGTTCTTCACCGACTTCCTC (Figure S2 and S3)	Eurofins MWG	N/A
mGAPDH Forward GGGAAATTCACGGCACAGT (Figure S2 and S3)	Eurofins MWG	N/A
mGAPDH Reverse AGATGGTGATGGGCTTCCC (Figure S2 and S3)	Eurofins MWG	N/A
Control siRNA (Cat# sc-108727) (Figure 7 and S8)	Santa Cruz Biotechnologies	N/A
siRNA anti human p57 (Cat# sc-37751) (Figure 7 and S8)	Santa Cruz Biotechnologies	N/A
Lgr5 promoter E-box Biotinylated in 5' or 3': CACTTAAGATGAAAAGTCCCTGGAAGTTAGCAAACAGCCATCTGCTACTCT GGCATCGATTTACTAAAAGTGACTTCTAG (Figure 7 and S8)	Eurofins MWG	N/A
Lgr5 promoter E-box reverse: CTAGAAGTCACTTTTAGTAAATCGATGCCAGAGTGACAGATGGCTGTTTGC TAACTTCCAGGGACTTTTCATCTTAAGTG (Figure 7 and S8)	Eurofins MWG	N/A
Mutant E-box Biotinylated in 5' or 3' (mutations underlined): CACTTAAGATGAAAAGTCCCTGGAAGTTAGCAAACAGCT <u>ATCAAT</u> CACTCA <u>AG</u> CATCGATTTACTAAAAGTGACTTCTAG (Figure 7 and S8)	Eurofins MWG	N/A
Mutant E-box reverse (mutations underlined): CTAGAAGTCACTTTTAGTAAATCGATGCT <u>TTGAGTGAT</u> <u>AG</u> CTGTTTGC AACTTCCAGGGACTTTTCATCTTAAGTG (Figure 7 and S8)	Eurofins MWG	N/A
Lgr5 Forward TCTCCCAGGTCTGGTGTGTT (Figure 7 and S8)	Eurofins MWG	N/A
Lgr5 Reverse AGTCCACCCTGAGCAACATC (Figure 7 and S8)	Eurofins MWG	N/A
Sox9 Forward GTAAACTCGGCTACGCATTA (Figure 7 and S8)	Eurofins MWG	N/A
Sox9 Reverse CCACCTCCTCCGACATTTCTTT (Figure 7 and S8)	Eurofins MWG	N/A
EphB3 Forward GTCTTGTCATTGCGGTAG (Figure 7 and S8)	Eurofins MWG	N/A
EphB3 Reverse CACTGGGCTGCGTATTTAG (Figure 7 and S8)	Eurofins MWG	N/A
Intergenic region Forward ATGGTTGCCACTGGGGATCT (Figure 7 and S8)	Eurofins MWG	N/A
Intergenic region Reverse TGCCAAAGCCTAGGGGAAGA (Figure 7 and S8)	Eurofins MWG	N/A



**Figure S1: Increased apoptosis in villi and increased proliferation in crypts of p57<sup>KO</sup> intestines. Related to Figure 1.**

Intestine sections of E18.5 p57<sup>+/+</sup>, p57<sup>KO</sup> and p57<sup>CK-</sup> embryos were stained for cleaved caspase 3 (A) or p57 and PCNA (B) to assess apoptosis and proliferation, respectively. DNA was stained with Hoechst 33342. p57<sup>KO</sup> intestine exhibit increased apoptosis in villi and increased proliferation in intervillous domains. This phenotype was never observed in p57<sup>CK-</sup> mutant mice. Scale bars: 50  $\mu$ m.



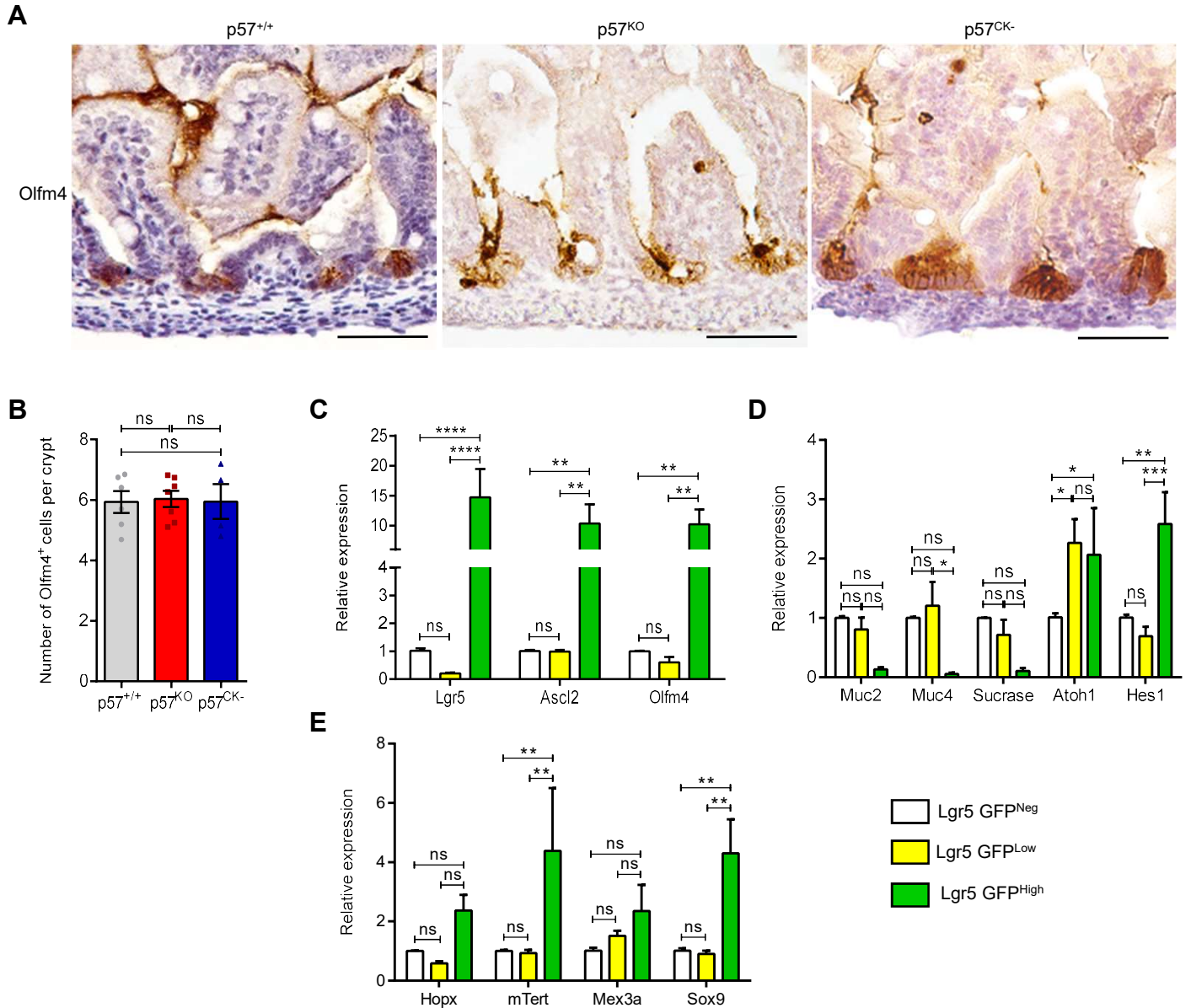


**Figure S2: Characterization of CBCs in p57 mutant mice.**

**Related to Figure 2.**

(A) Immunohistochemistry (brown) for the CBC marker Olfm4 in intestine sections from p57<sup>+/+</sup>, p57<sup>KO</sup> and p57<sup>CK-</sup> E18.5 embryos. Scale bars: 50  $\mu$ m. (B) Quantification of the number of Olfm4<sup>+</sup> cells per intervillous domain in p57<sup>+/+</sup> (n=6), p57<sup>KO</sup> (n=7) and p57<sup>CK-</sup> (n=4) intestines as described in A. Graph shows means  $\pm$  SEM. One-way ANOVA ns: p > 0.05. (C-E) Verification of the molecular identity of CBCs by RT-qPCR on sorted intestinal epithelial cells. Dissociated crypts from Lgr5<sup>+/e</sup>GFP-CreERT intestines were sorted based on GFP expression and gene expression of known CBC (C), differentiation (D) and reserve ISC (E) markers was evaluated in Lgr5 GFP<sup>Neg</sup>, Lgr5 GFP<sup>Low</sup> and Lgr5 GFP<sup>High</sup> populations (n=3). Expression levels were normalized to GAPDH expression and expressed relative to expression in GFP<sup>Neg</sup> cells. Graphs show means  $\pm$  SEM. Data were compared using one-way ANOVA ns: p > 0.05; \*: p  $\leq$  0.05; \*\*: p  $\leq$  0.01; \*\*\*: p  $\leq$  0.001; \*\*\*\*: p  $\leq$  0.0001.

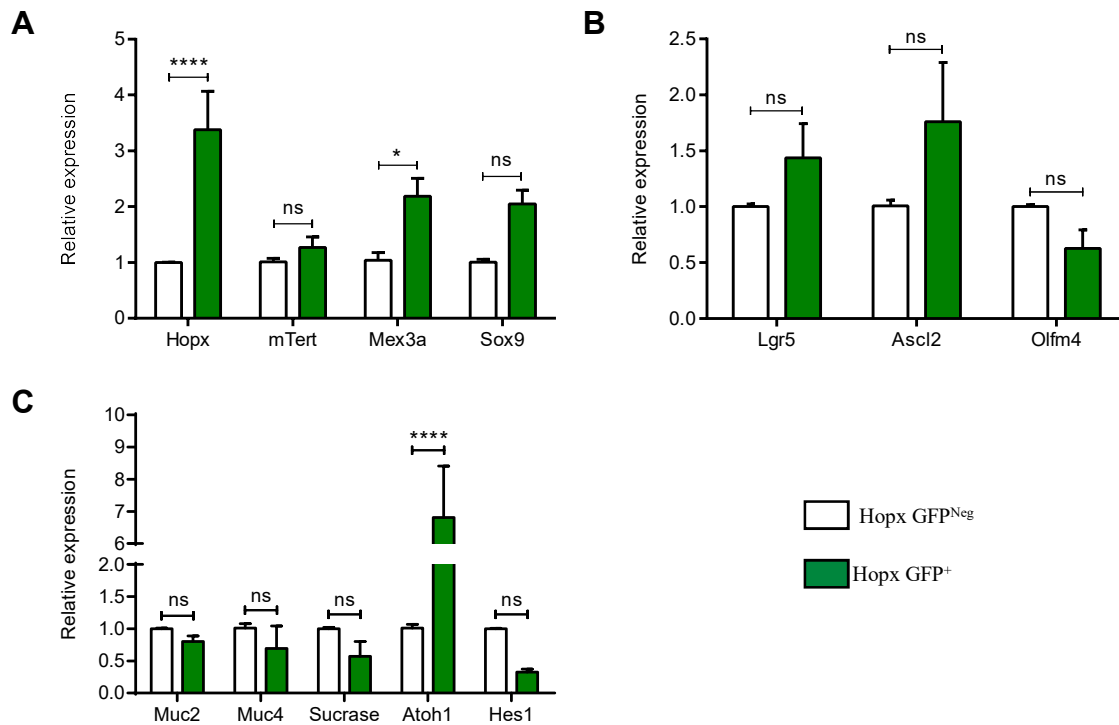


**Figure S3: Characterization of Hopx<sup>+</sup> ISCs in p57 mutant mice.**

**Related to Figure 3**

(A-C) The molecular identity of Hopx<sup>+</sup> ISCs was verified by RT-qPCR on sorted intestinal epithelial cells. Dissociated crypts from Hopx<sup>3Xflag-eGFP</sup> intestines were sorted based on GFP expression and gene expression of known markers of reserve ISCs (A), CBCs (B) and differentiation (C) was evaluated in Hopx-GFP<sup>Neg</sup> and Hopx GFP<sup>+</sup> populations (n=3). Expression levels were normalized to GAPDH expression and expressed relative to expression in GFP<sup>Neg</sup> cells. Graphs show means ± SEM. Data were compared using one-way ANOVA ns: p > 0.05; \*: p ≤ 0.05; \*\*\*\*: p ≤ 0.0001.

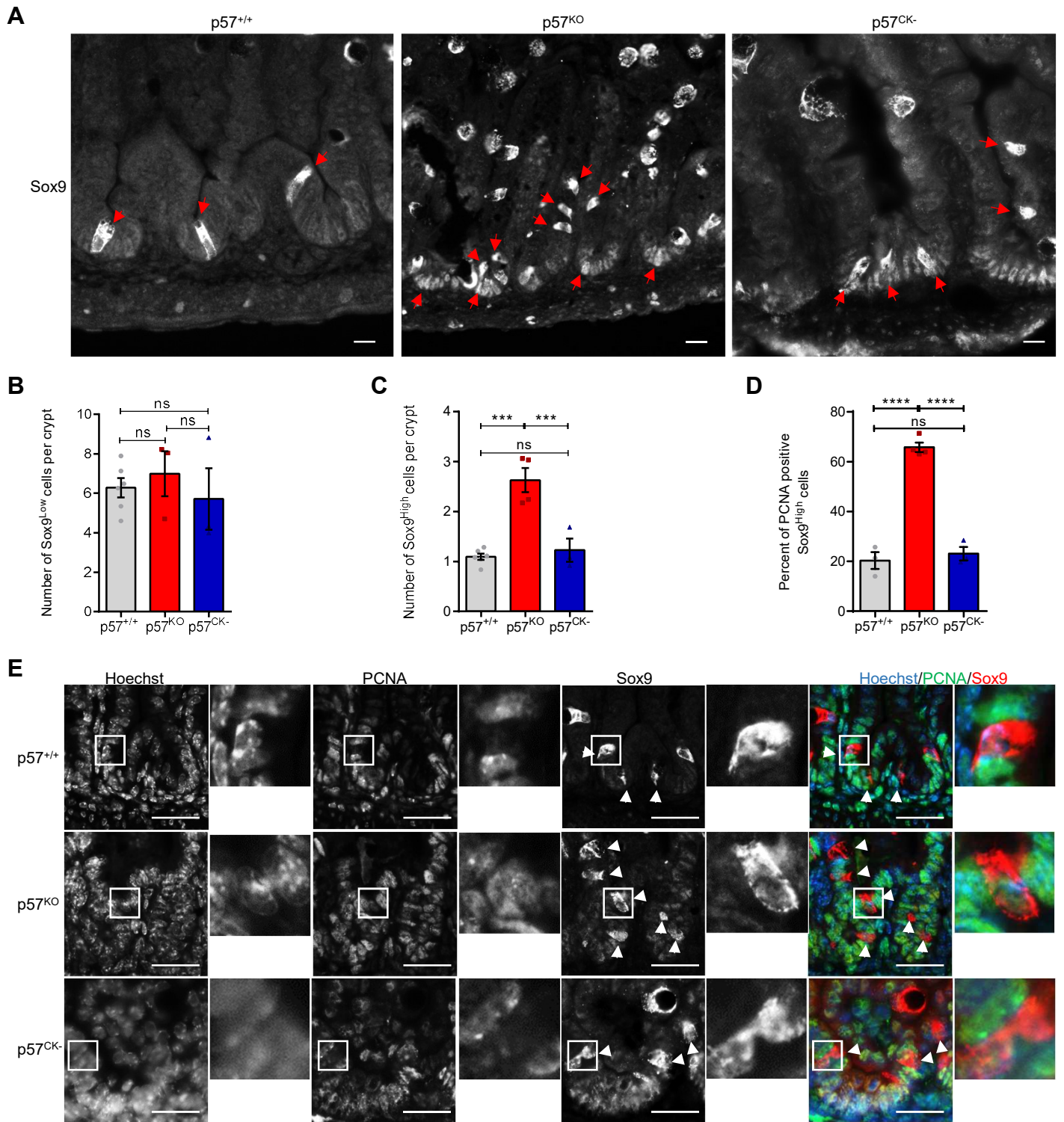


**Figure S4: Amplification of proliferative of Sox9<sup>High</sup> cells in p57<sup>KO</sup> intestines.**

**Related to Figure 3.**

(A) Intestine sections from p57<sup>+/+</sup>, p57<sup>KO</sup> and p57<sup>CK-</sup> E18.5 embryos were immunostained for Sox9. CBCs express low levels of Sox9 while reserve ISC express high levels of Sox9 (arrowheads). Goblet cells also exhibit high Sox9 expression but can be distinguished from reserve ISCs by their distinct morphology. Scale bars: 50  $\mu$ m. (B-C) Quantification of Sox9<sup>Low</sup> (B) and Sox9<sup>High</sup> (C) cells per intervillous domain in p57<sup>+/+</sup> (n=6), p57<sup>KO</sup> (n=3) and p57<sup>CK-</sup> (n=3) E18.5 intestines as described in A. (D) Percentage of proliferating Sox9<sup>High</sup> cells in intestinal sections immunostained for Sox9 and PCNA from p57<sup>+/+</sup> (n=3), p57<sup>KO</sup> (n=3) and p57<sup>CK-</sup> (n=3) E18.5 embryos, as shown in E. Graphs show means  $\pm$  SEM. one-way ANOVA ns:  $p > 0.05$ ;\*\*\*:  $p \leq 0.001$ ;\*\*\*\*:  $p \leq 0.0001$ . (E) Representative images of Sox9 and PCNA immunostaining of E18.5 intestine sections from p57<sup>+/+</sup>, p57<sup>KO</sup> and p57<sup>CK-</sup> E18.5 embryos. Sox9<sup>High</sup> cells are indicated by arrowheads. DNA was stained with Hoechst 33342. Scale bars: 20  $\mu$ m.

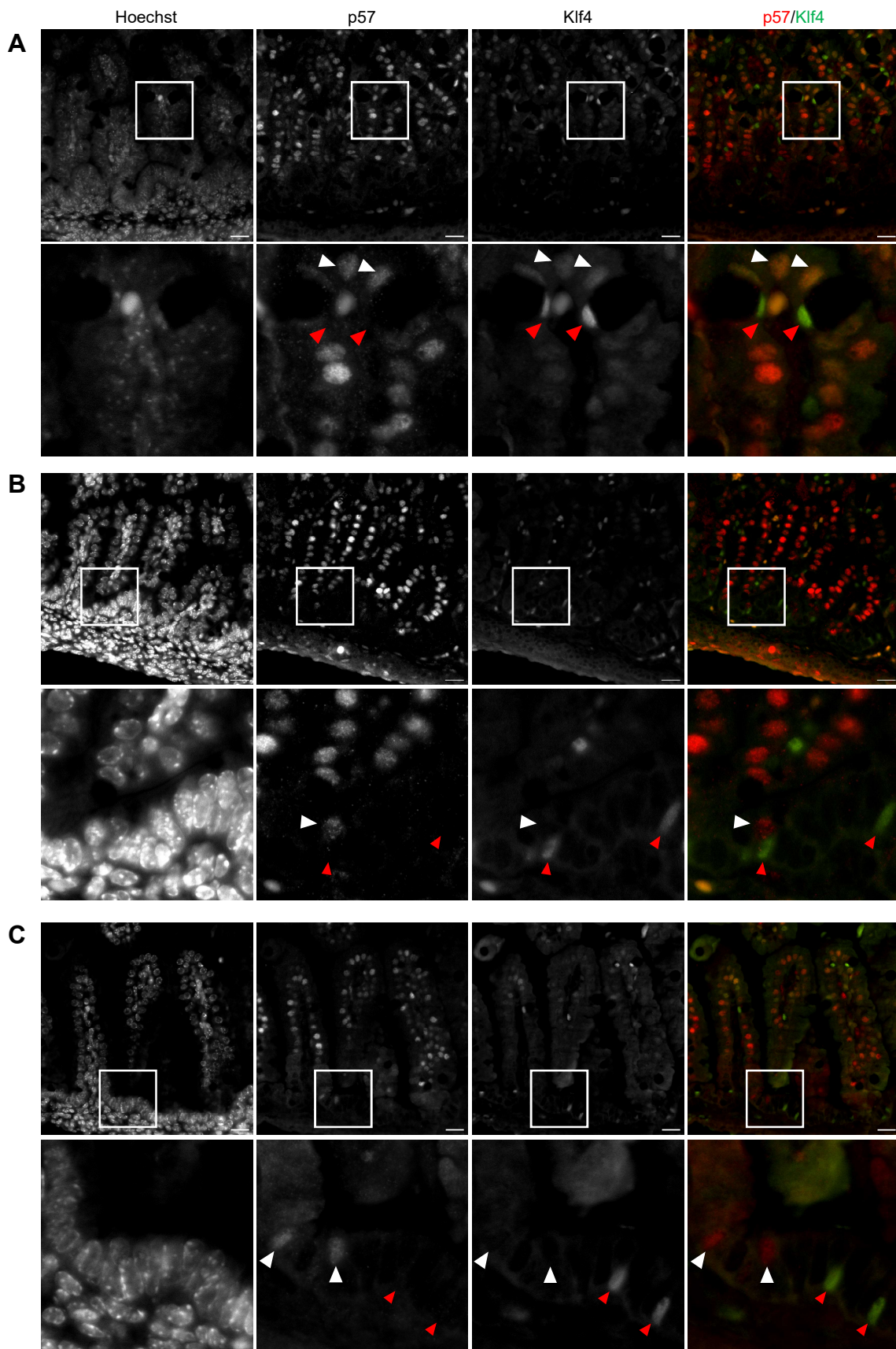


**Figure S5: Klf4 and p57 do not colocalize in the progenitor compartment.**

**Related to Figure 3.**

Paraffin embedded intestine sections of E18.5  $p57^{+/+}$  embryos were immunostained for p57 (red) and Klf4 (green) to assess colocalization. DNA was stained with Hoechst 33342. (A) p57 and Klf4 colocalize in some terminally differentiated cells in villi (white arrowhead) and Klf4 (but not p57) is strongly expressed in goblet cells (red arrowhead). (B, C) p57 is expressed at/near the +4 position in crypts (white arrowhead), while Klf4 is expressed in distinct cells in the crypts (red arrowhead). Scale bars: 20  $\mu\text{m}$ .

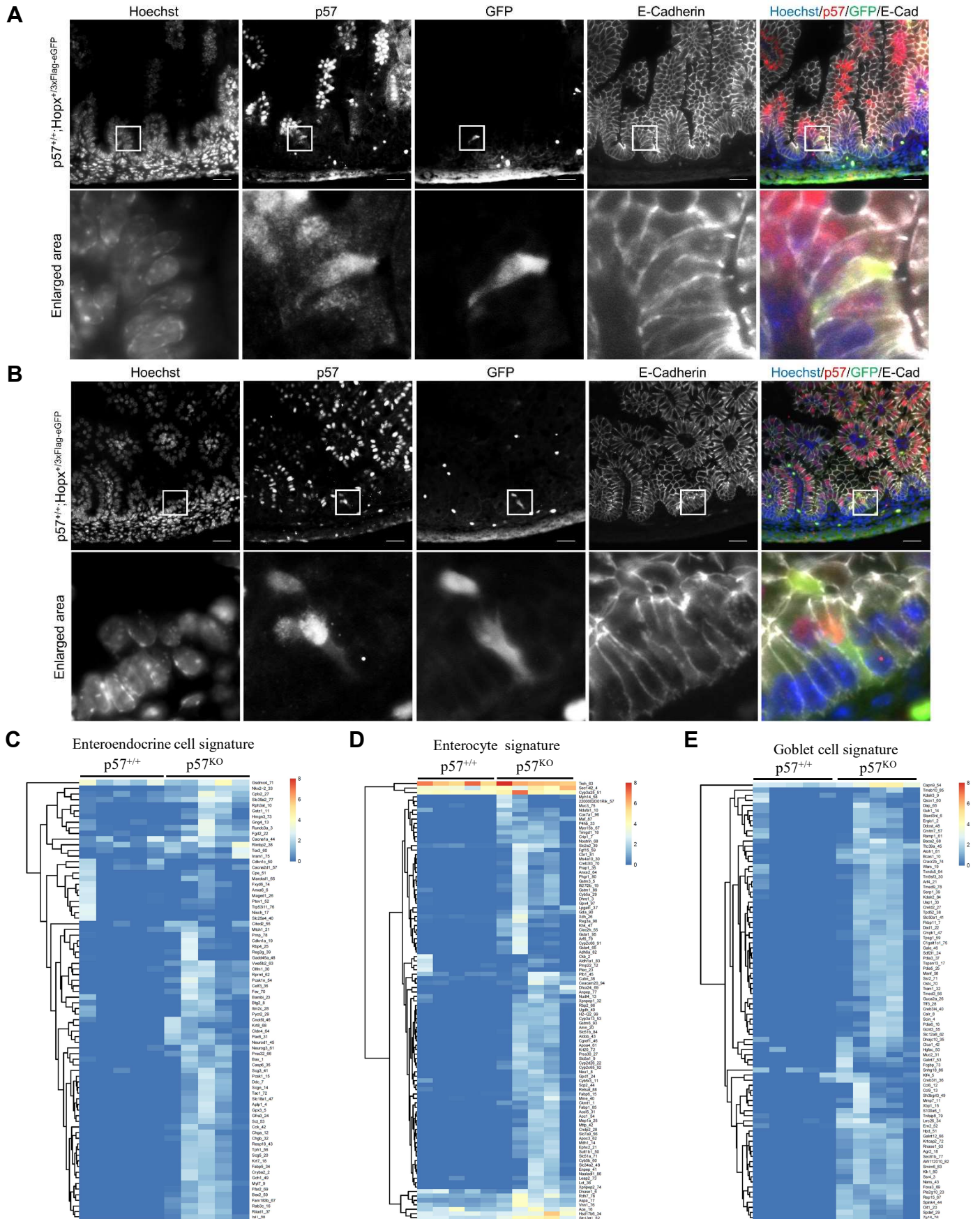


**Figure S6: Alteration of gene expression signatures in  $Hoxp^+$  ISCs of  $p57^{KO}$  mice. Related to Figure 4.**

(A, B)  $p57$  is expressed in  $Hoxp^+$  stem cells. Representative images of GFP,  $p57$  and E-Cadherin immunostaining of  $p57^{+/+};Hoxp^+/3xFlag-eGFP$  E18.5 intestines. DNA was stained with Hoechst 33342. Scale bars, 25  $\mu$ m.

(C-E) Heatmaps of  $Hoxp$ -GFP $^+$  ISC RNA-Seq analyses from  $p57^{+/+}$  ( $n=5$ ) and  $p57^{KO}$  ( $n=5$ ) mice for previously published gene expression signatures of specific intestinal cell populations: Enteroendocrine cells (C), Enterocytes (D), and Goblet cells (E).

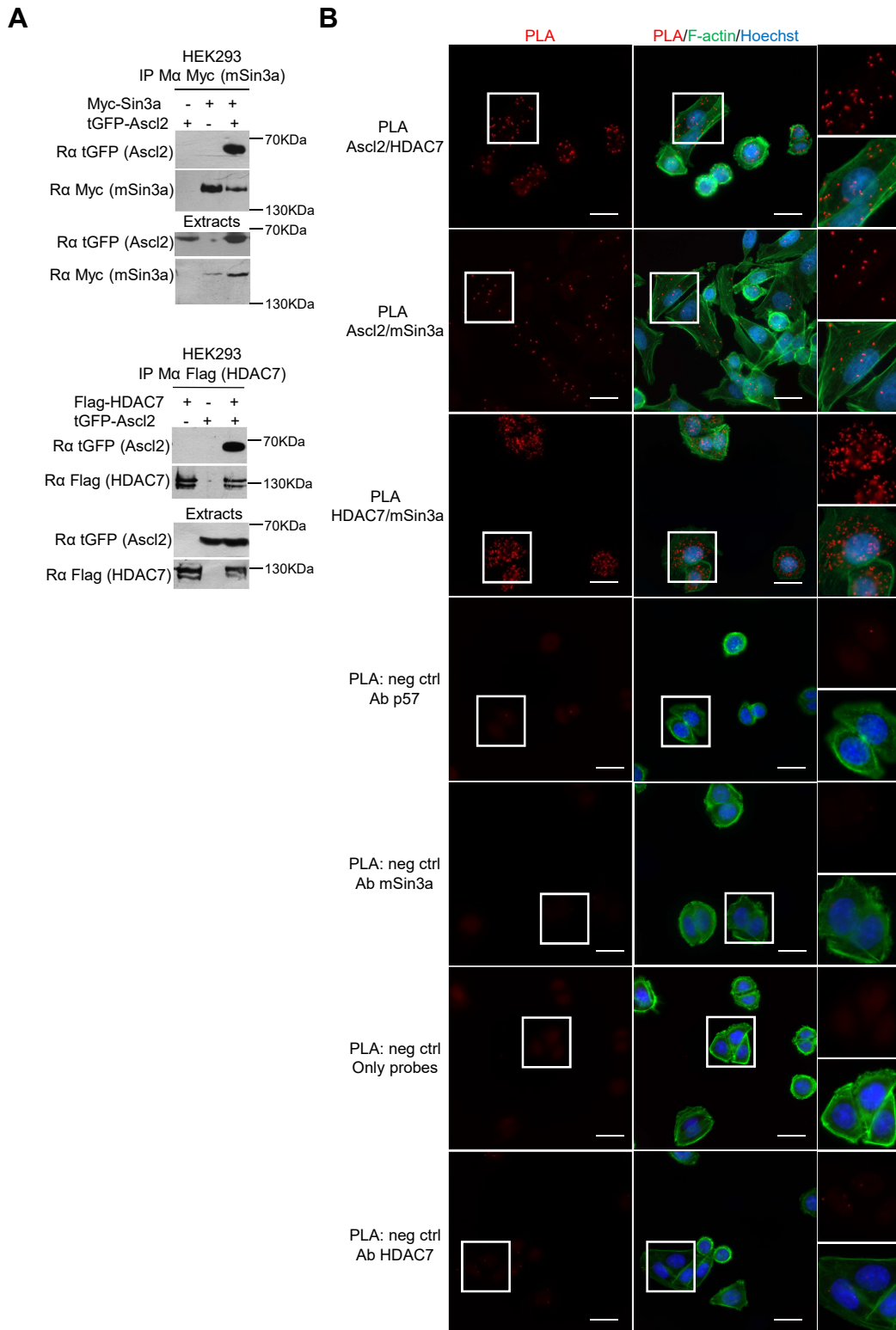


**Figure S7: Validation of the interaction partners of the corepressor complex. Related to Figure 6.**

(A) mSin3a or HDAC7 were immunoprecipitated with Myc or Flag antibodies, respectively, from HEK293 cells transfected with tGFP-Ascl2 and/or Myc-mSin3a and/or Flag-HDAC7. The presence of Ascl2 was assessed by immunoblotting with the indicated antibodies (n=3). Respective levels of transfected proteins in the extracts are shown. (B) PLA using Ascl2, mSin3a and/or HDAC7 antibodies on endogenous proteins in SW480 cells. F-actin was stained with phalloidin and DNA with Hoechst 33342. Scale bars: 50  $\mu$ m. Representative images of three independent experiments.

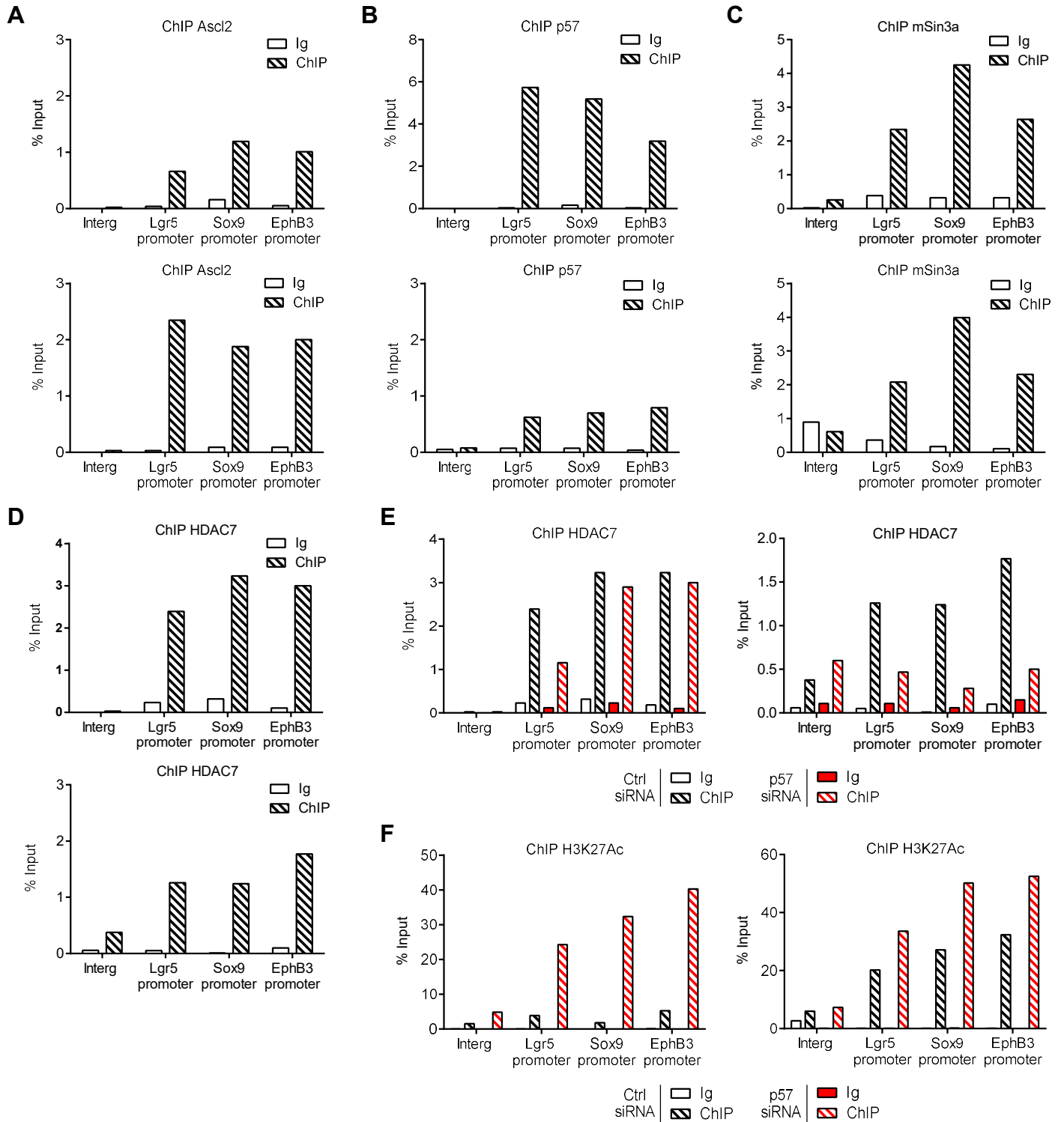


**Figure S8: p57 participate in the recruitment of a co-repressor complex on Ascl2 target promoters. Related to Figure 7.**

(A-F) Graphs show the results of two assays from three independent experiments, the third one is displayed in Figure 8. (A-D) ChIPs were performed with antibodies against Ascl2 (A), p57 (B), mSin3a (C), HDAC7 (D) or IgG as negative control to determine the presence of the co-repressor complex on Ascl2 target promoters. (E-F) ChIPs with anti HDAC7 (E) or H3K27Ac (F) antibodies or control IgG in SW480 cells transfected for 48 h with control or p57 siRNA followed by qPCR with primers specific for the Lgr5, Sox9 and EphB3 promoters or for an unrelated intergenic region as negative control.